Deep–Sea Research I 212 (2024) 104374

Contents lists available at ScienceDirect

Deep-Sea Research Part I

journal homepage: www.elsevier.com/locate/dsri

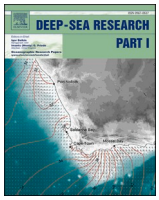

Census and properties of mesoscale eddies in the Kuril Basin of the Okhotsk Sea

Aleksandr Udalov, Maxim Budyansky, Sergey Prants *, Aleksandr Didov

V.I. Il'ichev Pacific Oceanological Institute, FEB RAS, 43 Baltiyskaya St., Vladivostok, Russia

ARTICLE INFO

Keywords:
Okhotsk Sea
Mesoscale eddies
Eddy detection
Kinematic characteristics
Core water origin

ABSTRACT

High spatial-resolution satellite images show the presence of numerous eddies in the deep Kuril Basin of the Okhotsk Sea, where in-situ measurements acquired within eddies are relatively rare. We conducted the first altimetry-based systematic census of mesoscale eddies in the Kuril Basin in 1993–2021 using the automatic eddy tracking algorithm AMEDA. The dominance of cyclonic eddies over anticyclonic eddies was observed, which contradicts the common opinion that anticyclonic eddies prevail over cyclonic ones in the Kuril Basin. The paper focuses mainly on the long-lived eddies with the lateral size in the range from several tens of kilometers to some hundreds of kilometers and with the lifetime exceeding 30 days. It was found that these eddies are inhomogeneously distributed over the study area with high values of occurrence frequency in some domains. This is explained by the topographic features and peculiarities of the circulation in the Basin where Soya Warm Current water, Okhotsk Sea water and subarctic Pacific water circulate and mix. The fractions of these water masses and their seasonal and interannual variations within the surface cores of the eddy were estimated using a particle-tracking technique. The kinematic characteristics of these eddies have been computed as well. The vast majority of the anticyclonic and cyclonic eddies have the nonlinearity parameter exceeding one implying that the eddies in the Kuril Basin are coherent features transporting water with its properties. Peculiarities in distribution of formation, occurrence and decay locations have been analyzed. Our results have been compared with shipboard and buoy's observations and numerical simulation of eddies in the Kuril Basin.

1. Introduction

The Okhotsk Sea (OS) is the largest marginal sea in the Pacific Ocean (Fig. 1) and an important source of ventilation of the North Pacific intermediate water (e.g., Talley, 1991; Shcherbina et al., 2003). It is connected with the subarctic gyre of the Northwestern Pacific and separated from the ocean by the Kuril Islands chain. The OS is connected with the Japan Sea through the Soya/La-Perouse and Nevelskoy straits. The exchange through the narrow Nevelskoy Strait is negligible. The surface circulation is generally cyclonic in the central and northern basins of the OS with the West Kamchatka and East Sakhalin currents as the prominent features of this circulation (e.g., Ohshima et al., 2002; Ebuchi, 2006; Fayman et al., 2021). In contrast with the Kuril Basin (KB) in the southern part of the Sea, the central basin appears quiescent, both in the mean and eddy kinetic energies. The overall flow field in the KB with the maximum depth of 3916 m, that is located on the pathway of the ventilated water from the OS, is a seasonal anticyclonic gyre that peaks in late summer (Wakatsuchi and Martin, 1991; Mensah and Ohshima, 2020). The first baroclinic Rossby radius of deformation in the OS has been estimated by Stepanov (2017) using the hydrological dataset from the World Ocean Atlas 2001 and 2013. It is maximum over the KB (18–20 km), minimal over the northern shelf (1.5–2 km) and intermediate in the central part of the Sea (8–10 km).

The deep KB is a region where three water masses mix to form the OS intermediate water: the Soya Warm Current water, the subarctic water, and the dense shelf water. The Soya Warm Current carries warm and saline water from the Japan Sea that flows into the KB mostly during summer. The water of this current flows out of the OS into the ocean through the southernmost Kuril straits. The saline and relatively warm subarctic water flows into the OS mainly through the central and northern straits (e.g., Katsumata and Yasuda, 2010; Fayman et al., 2021). This water is transported by the offshore branch of the East Sakhalin Current but does not reach the KB before May (Shcherbina et al., 2003; Gladyshev et al., 2000; Nihashi et al., 2009). Some areas in and around the KB are known as favorable fishing grounds, especially for walleye pollock (Budyansky et al., 2022a; Kolonchin et al., 2022;

* Corresponding author.
E-mail address: prants@poi.dvo.ru (S. Prants).

https://doi.org/10.1016/j.dsr.2024.104374
Received 26 August 2023; Received in revised form 29 July 2024; Accepted 9 August 2024
Available online 10 August 2024

Mundo et al., 2023). So, the knowledge of the oceanographic features, including mesoscale eddies, and their impact on the primary productivity in the area is important for sustainable fishery.

By the common opinion, the KB is populated mainly by anticyclonic eddies (AEs) with a diameter of 100–200 km that can affect the mean circulation and structure of the waters in the Basin. They are easily revealed from space as spiral structures in ice floe patterns, with the help of surface drifters and satellite imagery (Wakatsuchi and Martin, 1990; Khen and Muktepaveln, 1995; Thomson et al., 1997; Ohshima et al., 2002; Rabinovich et al., 2002; Zhabin and Luk'yanova, 2011; Mitnik and Dubina, 2019; Zhabin and Andreev, 2019). Just a few AEs have been sampled in cruises (Wakatsuchi and Martin, 1990, 1991; Rogachev, 2000). Some AEs in the southern/western KB were found to have cold cores, originating from the East Sakhalin Current water, whereas the others had warm cores, originating from the Soya Warm Current water (Wakatsuchi and Martin, 1991; Shevchenko et al., 2020). The eddy energy has been estimated to be much larger than the mean energy in the KB, based on surface drifter data and numerical simulation (Ohshima et al., 2002; Ohshima et al., 2005). These eddies may favor the formation of the OS intermediate water via lateral mixing (Mensah et al., 2019).

Some attention has been paid to the mechanism of formation of AEs in the OS in the area adjacent to the Kuril Straits. It was hypothesized by Nakamura and Awaji (2004), and then it has been shown by Ohshima (2005) with a simple numerical model, that anticyclones can be produced by baroclinic instability associated with a front in this area between relatively uniform water with low potential vorticity and offshore water. Available potential energy can be produced at this front being an energy source for baroclinic instability. The very strong tidal mixing in the Kuril Straits causes the baroclinic instability, resulting in regular generation of eddies along the seaside of the Kuril Straits (Ohshima et al., 2005). These eddies propagate westward and new eddies are subsequently produced near the Straits. With the inclusion of the surface-layer restoring in the model, only AEs with concave isopycnals at mid-depth tend to survive, since cyclonic eddies (CEs) with convex isopycnals near the surface are damped due to the surface restoring.

The present paper is aimed to fill a gap in the knowledge about the mesoscale eddies in the KB. By KB eddies, we mean here the eddies which spent at least 30 days in the area deeper than 3000 m that is conventionally considered as the KB boundary. With this aim, we plan (1) to provide the first systematic census of AEs and CEs in the KB in altimetry era (1993–2021); (2) to calculate and analyze the eddy kinematic characteristics and properties; (3) to estimate fractions of different water masses within the surface cores of the KB eddies; (4) to compare our results with shipboard and buoy's observations and numerical simulation of eddies in the KB.

Section 2 introduces the automated tracking algorithm for detection of eddies, Lagrangian methods and the data sources that we used in the present paper. Section 3 contains the main results including a census and the spatial distribution of KB eddies in 1993–2021, kinematic characteristics and properties, and calculation of the composition and origin of water within eddy cores during this period of time, including their interannual and seasonal variability. The results obtained are discussed in Section 4. Conclusions are provided in Section 5.

2. Data and methods

2.1. The angular momentum eddy detection and tracking algorithm

Mesoscale eddies with the size exceeding 50 km are reliably identified in the altimetric velocity field (one of the AVISO/CMEMS products, aviso. altimetry.fr) with the resolution of 0.25° × 0.25° and daily time step. This product uses corrections for changes in sea level caused by various hydrometeorological phenomena (tides, changes in atmospheric

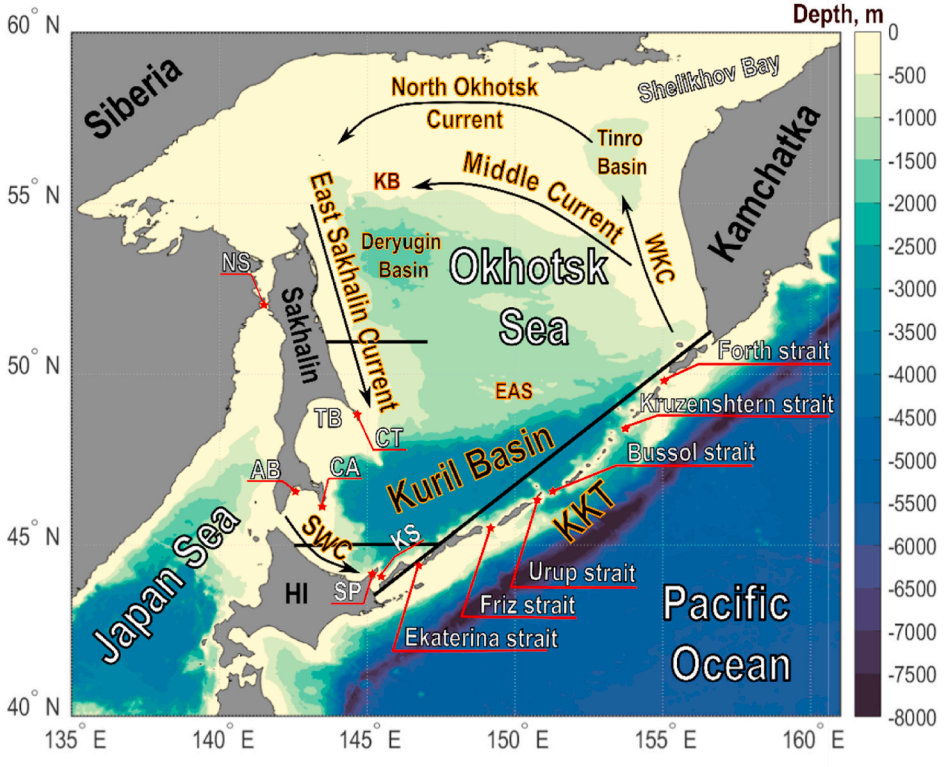

Fig. 1. Bathymetry of the Okhotsk Sea, schematic of the main currents and some geographical features. The straight segments are used to distinguish the origin of water in the Kuril Basin and within the surface cores of the long-lived eddies there (see Fig. 9 and Sec. 3.2.2). WKC is West Kamchatka Current. KKT is for Kuril-Kamchatka Trench. NS and KS stand for the Nevelskoy and Kunashir straits, respectively. HI – Hokkaido Island, TB and AB – Terpeniya and Aniva bays. SP – Shiretoko Peninsula. CA and CT – Cape Aniva and Cape Terpeniya. EAS and KB stand for Elevation of Academy of Sciences and Kashevarov bank.

pressure, etc.), but not by pack ice cover. The ice concentration data from the EUMETSAT Ocean and Sea Ice Satellite Application Facility – Global Sea Ice Concentration Data Record [OSI SAF, www.osi-saf.org] indicate that the KB is practically ice-free all year round with some small areas with floating ice in severe winters (see also Kolomeytsev, 2020). This allows us to use the AVISO data for geostrophic currents. For the statistical studies, we use this product from 28-year altimetric sea level records at one frame per day, from January 1, 1993 to December 31, 2021.

To detect eddies, we apply the Angular Momentum Eddy Detection and tracking Algorithm (AMEDA https://github.com/briaclevu/AMEDA) (Le Vu et al., 2018). Firstly, the eddy's centers are identified, which correspond to an extremum of the local normalized angular momentum with the value of 1 and -1 for cyclonic and anticyclonic eddies, respectively. The streamlines surrounding this center are then computed. The local Okubo-Weiss parameter is used to confirm that the detected eddy center is in a vorticity-dominated region of the flow. Finally, to ensure that the extremum of the local normalized angular momentum is indeed an eddy center, the algorithm keeps the extremum only if there exist closed streamlines around it. The mean radius <R> and the mean swirl velocity <V> are computed along each closed streamline. This mean radius <R> is defined as the equivalent radius of a disc with the same area S as the one delimited by the closed streamline, while the mean swirl velocity <V> is derived from the circulation along the closed streamline (Stegner et al., 2021). The characteristic radius R_{max}, at which a maximum swirl velocity V_{max} is reached, is used to quantify the eddy size. The characteristic contour of the detected eddy is associated with the closed streamline of the maximal swirl speed. This contour approximately defines the lateral extent of the surface core of an eddy.

When identifying merging and splitting of eddies, the area of interaction of two eddies is determined by finding a contour around them. The algorithm also tracks the movement of eddies before and after the interaction. Thus, a merger event is realized if one of the eddy's trajectories ends up after interaction. Splitting event is realized if there was only one trajectory before interaction. AMEDA provides information about the formation sites of eddies, that can be recognized from the merger/splitting tree.

The algorithm is robust to the grid resolution, uses a minimal number of tunable parameters and provides a complete dynamical evolution of the detected eddies during their lifetime. In contrast with the algorithm of Chelton et al. (2011) and the META3.2 algorithm (Pegliasco et al., 2022), AMEDA allows us to identify merger and splitting of eddies that is crucial for the census of eddies and gives a more realistic estimate of the area of the identified eddies. The efficiency of AMEDA was tested by Le Vu et al. (2018) and Stegner et al. (2021) with three different types of input data: the 1/8° AVISO geostrophic velocity fields available for the Mediterranean Sea; the output of the ROMS numerical model and the surface velocity field obtained from particle imagery in a rotating tank experiment. It has been also verified with Aleutian eddies by Budyansky et al. (2022b) and trench eddies by Udalov et al. (2023).

2.2. Lagrangian methods

In the altimetry-based Lagrangian approach, one computes trajectories for a significant number of virtual passive particles in the AVISO velocity field solving the two-dimensional advection equations which are represented in the simplest form as follows:

$$\frac{d\lambda}{dt} = u(\lambda, \varphi, t), \frac{d\varphi}{dt} = v(\lambda, \varphi, t), \quad (1)$$

where φ and λ are latitude and longitude of particle's location, u and v are the angular zonal and meridional geostrophic velocity components at the location of a particle.

The altimetric velocity field is given on the 0.25° × 0.25° grid with the daily time step. To integrate the advection equations, we need to interpolate discrete velocity data to a continuous function in space and time. We use two methods: a bicubic interpolation in space and a simultaneous linear interpolation in time with third-order Lagrangian polynomials. A linear spatial interpolation is insufficient since it ensures the continuity of the interpolating function when crossing the grid cell boundaries, but its derivatives are discontinuous at these boundaries. The bicubic interpolating function has 16 coefficients, but that enables us to get more accurate results. The interpolation in time is much simpler than the spatial one, since we are dealing with a one-dimensional function. It has been demonstrated by Mancho et al. (2006) for chaotic flows that the bicubic spatial interpolation together with third-order Lagrange polynomials in time give excellent accuracy at very modest computational expense compared to other methods.

The particle's trajectories were computed by integrating equation (1) using the 4th order Runge-Kutta scheme (for details see Prants, 2015; Prants et al., 2017). The angular velocity is related to the linear velocity by the ratio (Prants et al., 2022)

$$u = \frac{0.864}{1.853}\frac{1}{\cos\varphi}U, v = \frac{0.864}{1.853}V \quad (2)$$

where u and v are expressed in arc minutes per day, and U and V are given in cm/s.

To track the origin of water in the KB eddies, trajectories for hundreds of thousands of particles were computed backward in time. The water in the KB eddy cores could be, in general, a mix of waters originated from the open ocean subarctic water, Okhotsk Sea (East Sakhalin Current) and Japan Sea (Soya Warm Current). The area 39°–60°N, 135.5°–167°E in the OS was divided into a uniform grid of 760 × 720 nodes with particles, for each of which trajectories were calculated in reverse time. The water masses are distinguished in accordance with the segments, shown in Fig. 9, which were crossed by the particle's trajectories within the past 365 days. This integration time was empirically found to be enough to reach the remote regions in the KB. Each trajectory was stopped when it reached in the reverse time one of the segments, and the corresponding particle was depicted by color on the geographic map giving us a daily origin or O-map (Prants et al., 2018). Different colors on such maps represent the water masses mentioned above. As a result, a gallery of daily O-maps was obtained. The contours of the identified eddies were placed on each O-map every day. After that, the ratio of the number of particles within each contour, which crossed one of the three selected segments, to the total number of grid nodes within the considered contour was calculated. This approach makes it possible to calculate the daily value of the ratio of the number of markers, simulating waters of various origin, to the total number of markers within the contour as the eddy moves.

To compute the seasonal variations of the fractions of the open ocean, East Sakhalin Current and Soya Warm Current waters within the surface cores of the long-lived AEs and CEs in the KB, we created an array with 366 bins corresponding to every day of a leap year. Fractions of these water masses were calculated for each KB eddy every day during its lifetime and then averaged over all the eddies for each bin. The results are represented as time plots from the beginning of 1993 to the end of 2021 for AEs and CEs separately.

The fraction of each water mass changes during the eddy lifetime. To quantify that, we normalize the lifespan of different eddies as follows. For each long-lived KB eddy, the set n = 1, …, N, where n numerates the day of the eddy lifetime, maps onto the set n = 0, …, 1 with the same dimension. Each eddy has its own dimension which depends on its lifetime. The fraction of particles of a given origin is interpolated to the same grid from 0 to 1 with a step of 0.001 for each eddy. The dimension of the normalized time sets is now the same for all eddies. The fraction of each water mass is averaged over all the eddies for each normalized time interval to give time plots.

The algorithm, described above, has been used to calculate the

averaged fractions of the distinct water masses within the surface cores of long-lived AEs and CEs at different stages of their lifetime and TS diagrams, based on the data of the eddy-resolving reanalysis GLORYS12V1 with the horizontal resolution of 1/12° and 50 vertical levels. This product is available since 1993 at the website of CMEMS (https://data.marine.copernicus.eu/product/GLOBAL_MULTIYEAR_PHY_001_030/description). The reanalysis is based on the NEMO platform, in which *in situ* and satellite observations and data from drifting buoys are assimilated using the Kalman filter.

Profiling floats deployed in the OS as part of a joint Hokkaido University-University of Washington program were also used to identify the water properties within eddies detected by AMEDA. These data are made available by the Arctic Data archive System of the Japanese National Institute of Polar Research, https://ads.nipr.ac.jp/data/meta/A20240520-001.

3. Results

3.1. Census and spatial distribution of mesoscale eddies in the Okhotsk sea in 1993–2021

We consider each detected eddy during its lifetime, from formation to decay, as one occurrence. In case of a splitting event, two new eddies appear with the largest one having the number of the parent eddy. Without any lifespan constraint, 1634 AEs and 1659 CEs (in total 3293) were detected in the entire OS basin (see Table 1), whereas 1098 AEs and 1139 CEs (in total 2237) with the lifetime exceeding 30 days were detected. Among these, 243 AEs and 366 CEs (in total 609) with the lifetime exceeding 30 days were detected in the KB area restricted by the 3000 m isobath. In the entire OS basin, an approximate parity was found between AEs and CEs, when no constraint was imposed on the lifespan of the eddies. In the KB, we have found a significant asymmetry in the polarity of the detected long-lived eddies with cyclones prevailing over anticyclones (see Table 1).

The occurrence frequency for eddies in the whole OS without lifespan constraint is displayed in Figs. 2 and 3 for AEs and CEs, respectively, with superimposed formation and decay sites during the time of observation (from Jan 1, 1993 to Dec 31, 2021). To obtain these figures, the study domain was first mapped onto a $0.1^\circ \times 0.1^\circ$ grid. The contours of the eddies were identified daily for the period 1993–2021 on the interpolated velocity field. We then computed the number of occurrences in which each grid point was included within a vortex contour. This yielded Figs. 2 and 3, i.e., maps of the ratio of the number of days occupied by eddies over the total number of days during the observation period (10,592).

The map in Fig. 2 shows that AEs have been observed much more frequently in the southern OS. Besides the KB area, AEs occur frequently to the east off the Cape Aniva and in the northern part of the Terpeniya Bay of Sakhalin Island where the East Sakhalin Current goes around the Cape Terpeniya. The AE occurrence frequency is comparatively small along the Middle Current that follows the 500 m isobath in the northwestern direction and delivers the Pacific water to the northeastern shelf of Sakhalin where it immediately flows into the East Sakhalin Current (Fayman et al., 2021). An increased AE activity, as compared to the quiet regions of the OS, is observed as well in the area of the Bussol and Kruzenshtern straits, through which the Pacific water also inflows into the Sea, and over the Elevation of Academy of Sciences and Kashevarov Bank (see Figs. 1 and 2a). The CEs occur more frequently in the southern OS (Fig. 3), especially in the KB. In contrast with AEs, an increased occurrence frequency of CEs was observed over the Deryugin Basin. The areas with relatively high occurrence frequency of CEs outside the KB are located in the Aniva Bay and near the northern coast of Hokkaido.

As to formation sites (Fig. 2a and 3a), AEs and CEs are generated more often along the seaside of the Kuril Islands between the coast and 3000 m isobath. The formation sites are also accumulated along the 3000 m isobath and in the KB. The comparatively high density of the formation sites is observed along the eastern coast of Sakhalin, especially in its southernmost bays. In the most southern part of the OS, the high occurrence frequency with accumulation of formation sites is observed in the area of the Cape Shiretoko for AEs and to the west of it for CEs. The branch of the Soya Warm Current turns there to the northeast and flows into the KB, whereas the other branch follows along the coast and flows out into the ocean (Takizawa, 1982; Ebuchi et al., 2009). As to decay sites, they are distributed approximately over the same areas as the formation sites except for the area to the north of the Bussol Strait where the formation sites prevail over the decay sites (Figs. 2 and 3).

Table 1
The number of anticyclonic (AE) and cyclonic (CE) eddies in the entire Okhotsk Sea basin without lifespan constraint and with constraints of 30, 60 and 90 days and in the Kuril Basin with the lifetime exceeding 30 days.

	Okhotsk Sea				Kuril Basin
	≥0	≥30	≥60	≥90	
AE	1634	1098	829	591	243
CE	1659	1139	874	612	366

3.2. Long-lived Kuril basin eddies

In what follows, we focus on long-lived mesoscale eddies which spent 30 days and more in the KB. Such eddies can be reliably detected by the altimetry-based AMEDA algorithm and tracked with the help of Lagrangian maps. It should be noted that the KB eddies under study are not necessarily formed or decayed in the KB. Besides the eddies which formed in the KB, we consider also the eddies which formed outside the KB but entered the KB somewhere and spent 30 days or more in the KB. The occurrence frequency for the KB eddies has been computed as it was described in Sec. 3.1, and it is displayed in Figs. 4 and 5 for AEs and CEs, respectively.

After formation, long-lived AEs and CEs circulate mostly in the KB area conventionally restricted by the 3000 m isobath and seldom propagate into the central OS Basin (Fig. 6). The striking difference in the distribution of long-lived eddies, as compared to the eddies without lifespan constraint (see Figs. 2 and 3), is the lower density of the formation sites of the long-lived eddies in the area adjacent to the seaside of the Kuril Islands (compare Figs. 2 and 3 with Figs. 4 and 5). It means that eddies with the lifespan shorter than 30 days form and often decay in this area possibly due to tidal-induced baroclinic instabilities. Nine AEs, formed to the east off Terpeniya Bay over the depression with the depth between 1000 and 2000 m, were also able to penetrate into the KB.

The plots with complicated trajectories of the long-lived AEs and CEs in the KB with the superimposed formation and decay sites are plotted in Fig. 6. These plots demonstrate the areas with increased density of trajectories in accordance with Figs. 4 and 5. The long-lived AEs circulate mostly near the Bussol and Kruzenshtern straits, where the Pacific water enters the OS, and in the central KB, whereas CEs circulate mostly in the deepest regions of the KB.

3.2.1. Kinematic properties of long-lived Kuril basin eddies

In this section, we present histogram distributions of kinematic characteristics of long-lived AEs and CEs in the KB. Discussion of the obtained results will be presented in the next section. The histograms of the eddies' lifetime for the AEs and CEs are shown in Fig. 7a. Distributions of eddies in the KB by the months of formation and decay are shown in Fig. 2S in Supplementary material. The numbers of AEs and CEs, formed in the cold season (Nov–Apr), are 122 and 178, respectively, almost the same as in the warm season (May–Oct), 121 and 188, respectively. Among all the eddies, 44 AEs and 27 CEs have been observed with the lifetime exceeding 300 days (Fig. 7a).

The path covered by each long-lived eddy in the KB has been calculated starting from the appearance of the elliptic point at the eddy's

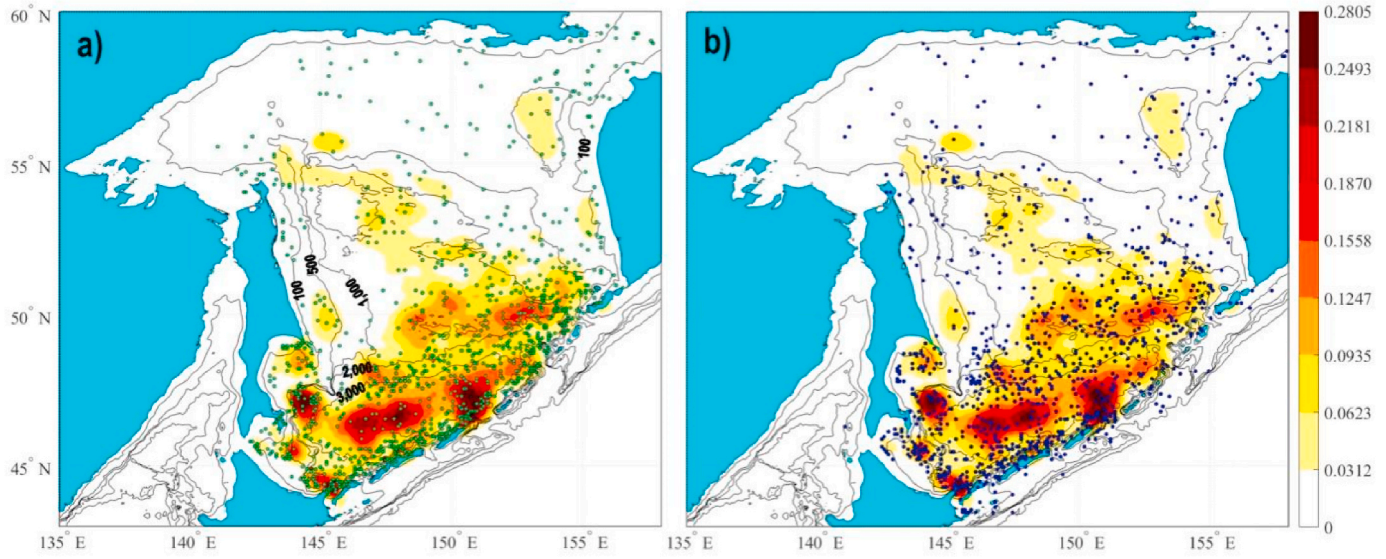

Fig. 2. The occurrence frequency of anticyclones in the Okhotsk Sea with superimposed a) formation (green dots) and b) decay sites (blue dots) without the constraint on the lifespan. The color scale in the bar highlights the locations with increased probability to observe anticyclonic eddies in 1993–2021. The isobaths of 100, 500, 1,000, 2000 and 3000 m are indicated.

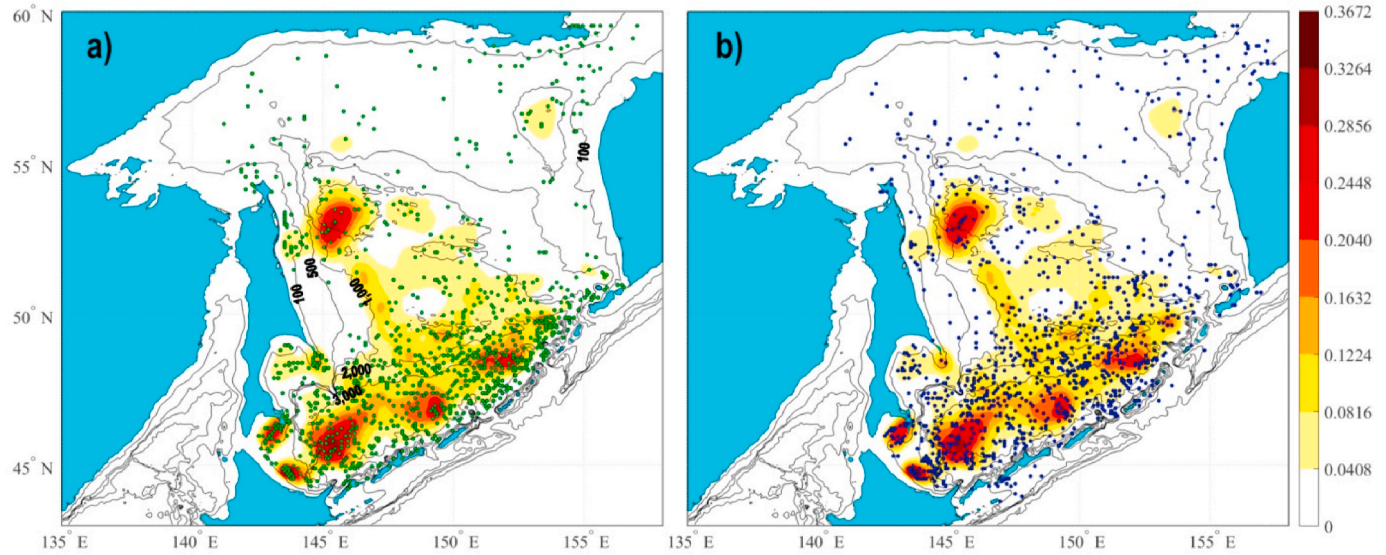

Fig. 3. The same as in Fig. 2 but for cyclones in the Okhotsk Sea.

center until eventual disappearance of this point. The histograms of the pass lengths of the long-lived AEs and CEs are plotted in Fig. 7b. To estimate to which degree eddies in the KB are coherent Lagrangian features, trapping water and its properties in their interior and transport them over great distances, the nonlinearity parameter has been computed for AEs and CEs separately. The nonlinearity parameter (Flierl, 1981; Chelton et al., 2011) is the ratio $\eta = V_{max}/c$. The histograms of the daily rotational speed of fluid, V_{max}, along the characteristic vortex contours for the long-lived mesoscale AEs and CEs are shown in Fig. 1S in Supplementary material. The larger the value of η for these eddies, the higher their nonlinearity. The nonlinear eddies are capable of transporting large volumes of water within the eddy interior that is advected with the eddy as it translates. Fig. 7c shows the histogram distributions of the long-lived AE and CE by the mean nonlinearity parameter. Among the observed AEs and CEs, 97.9% and 97.8%, respectively, were nonlinear eddies with $\eta > 1$. The histograms in Fig. 7d are the distributions of AEs and CEs by the intensity $<I> = <A>/<R_{max}>$ averaged during the eddy's lifetime.

The histograms in Fig. 8a and c display the distributions of the displacement of the eddy's center and the mean propagation speed. The displacement differs from the pathway length. Indeed, it is defined as the distance between the eddy's formation and decay sites on the Earth's sphere. The propagation speeds of AEs and CEs, averaged during the lifetime of each eddy, were distributed in the range from 1 to 10 km/day with the mean values equal to $<c> = 3.86$ km/day for AEs and $<c> = 4.48$ km/day for CEs. The histograms of distribution of the long-lived AEs and CEs in the KB by their mean area $<S>$ and mean radius $<R_{max}>$ are shown in Fig. 8b and d. The area of each eddy was calculated daily as the area within the characteristic contour S_i with the maximal rotational velocity of fluid parcels V_{max} around the eddy's center (see Sec. 2.1). The characteristic contour approximates a boundary of the surface vortex core. The mean area of an individual eddy is the arithmetic average of the areas of its daily characteristic contours during the eddy's lifetime. The difference in sea level anomaly

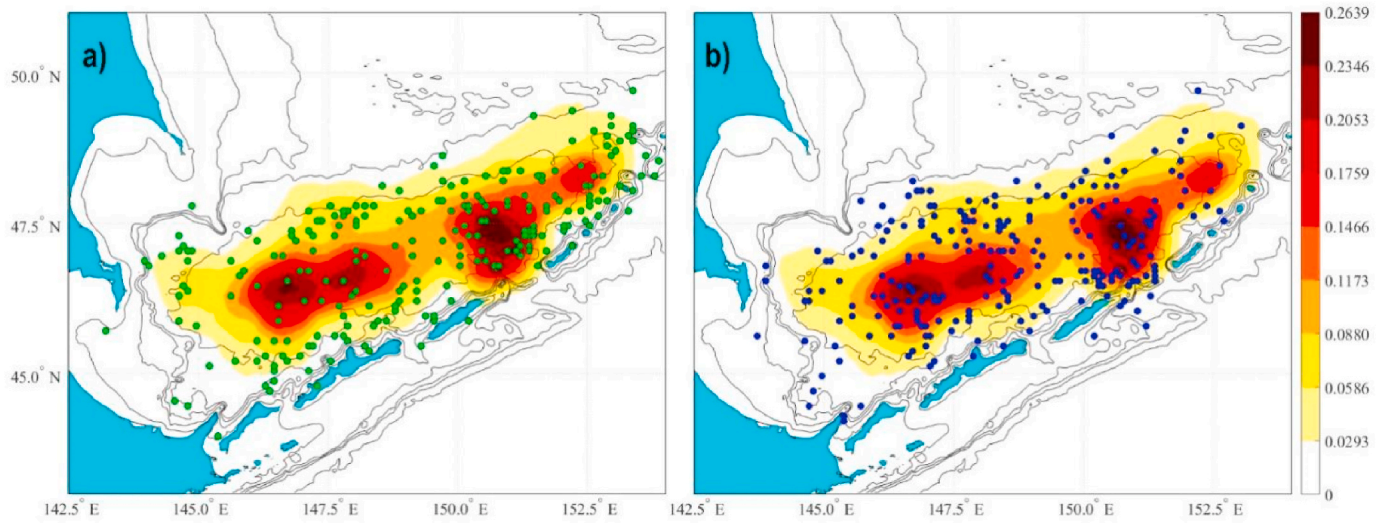

Fig. 4. The occurrence frequency of the long-lived anticyclones in the Kuril Basin existing there for 30 days and longer with the superimposed a) formation (green dots) and b) decay sites (blue dots).

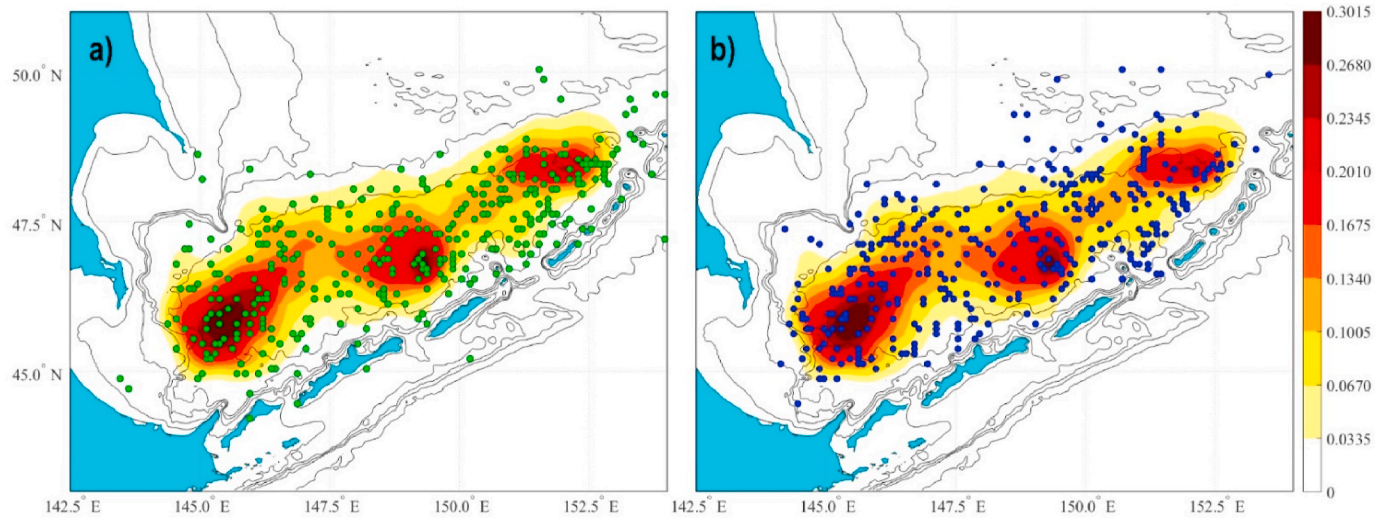

Fig. 5. The same as in Fig. 4 but for the long-lived cyclones in the Kuril Basin with the lifetime exceeding 30 days.

between the center and the edge of an eddy is defined as the amplitude of the eddy A.

3.2.2. Estimation of the fractions of different water masses within eddies

Three waters masses circulate and mix in the KB: the Soya Warm Current water originating in the Japan Sea, water of the offshore branch of the East Sakhalin Current and the Pacific water (see Fig. 1). The particle-tracking method described in Sec. 2.2 is used here to calculate the percentage of particles, simulating different water masses, within the surface cores of long-lived KB eddies. 547,200 particles were distributed at the nodes of the 760 × 720 grid covering the extended area (39–60°N, 135.5–167°E) that includes the whole OS and a part of the northwestern Pacific Ocean. The trajectory of each particle was calculated integrating advection equation (1) backward in time for one year. The integration was stopped when trajectories reached one of the segments shown in Fig. 9, which were chosen to cross the transport pathways of the Soya Warm Current, East Sakhalin Current and the subarctic Pacific water penetrating into the OS through the Kuril straits. The locations of these particles are depicted on the geographic map by different colors providing us with daily O-maps. There are also a comparatively small number of white particles of uncertain origin on the O-maps in the KB. The origin of these particles could not be determined either because they did not cross one of the selected segment or because a one-year integration time was not long enough to do that. The variations of the fractions of the surface open ocean, East Sakhalin Current and Soya Warm Current waters in the KB in 1994–2021 are shown in Fig. 10.

Using the algorithms described in Sec. 2.2, we computed seasonal variations of the fractions of these waters within the surface cores of the long-lived AEs and CEs in the KB. The corresponding plots are shown in Fig. 13a and b. The fractions of these water masses at different stages of the normalized eddy's lifetime are shown in Fig. 4S a and b, where the day of eddy's formation corresponds to 0 and the day of decay – to 1 on the x-axis. We did not observe significant variations of those fractions during the lifespan of AEs and CEs.

We compared the simulated results with actual data from the profiling floats deployed in the OS by selecting floats inside of a few long-lived AEs and CEs in different parts of the KB and in different seasons. With the aim of finding out whether the thermohaline properties really differ for eddies with various estimated fractions of the main

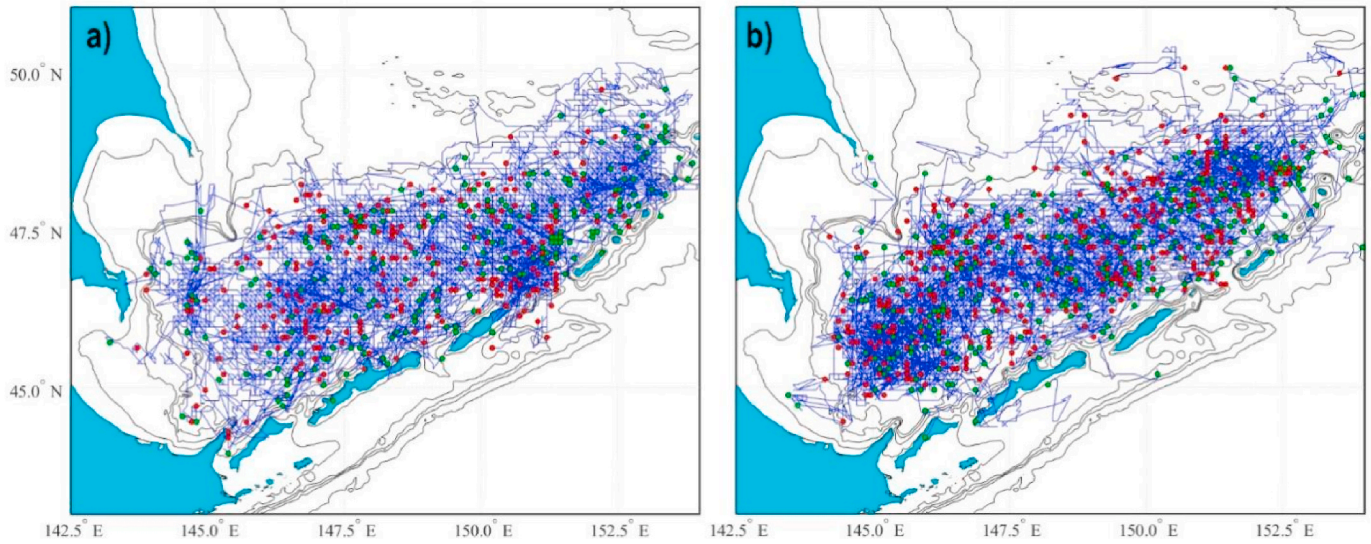

Fig. 6. Trajectories of the long-lived a) anticyclones and b) cyclones in the Kuril Basin with the superimposed formation (green dots) and decay sites (red dots).

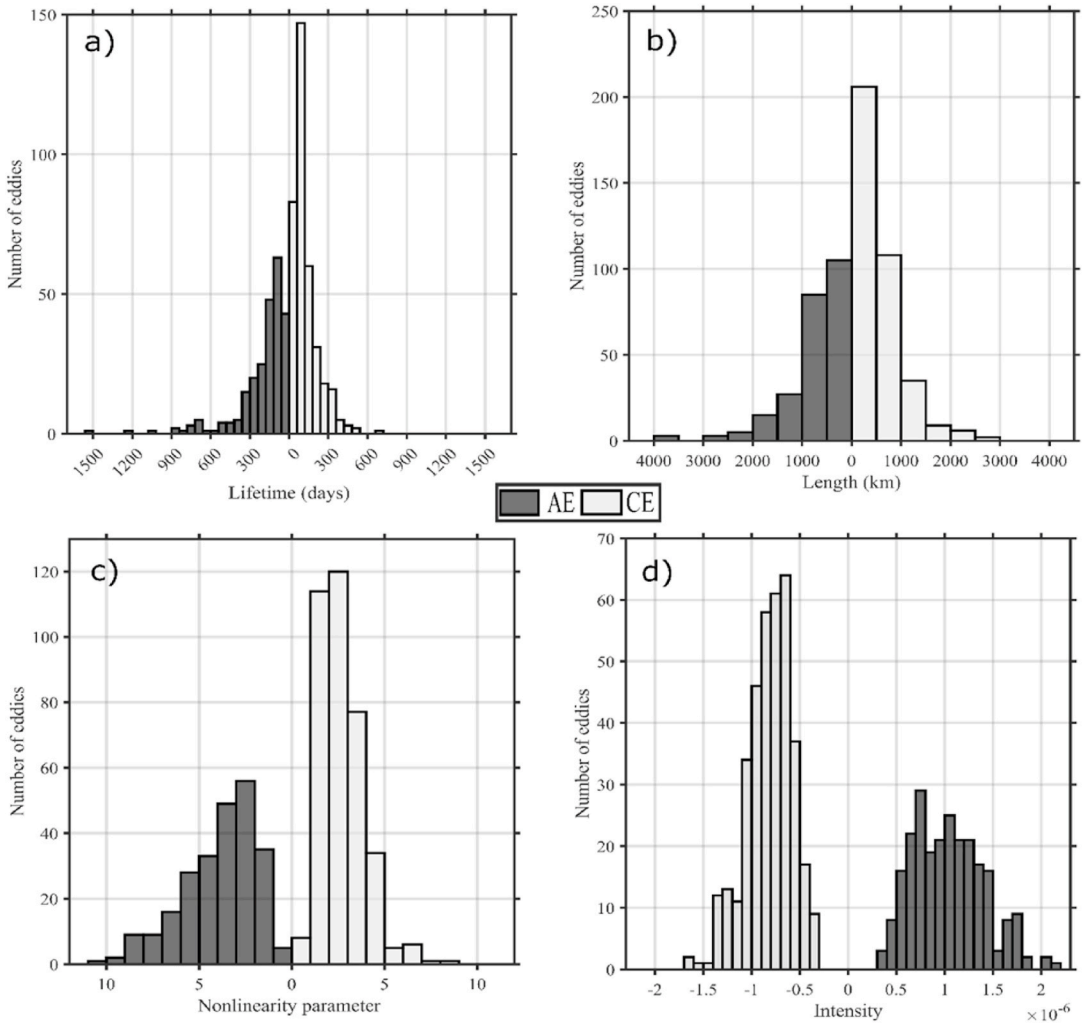

Fig. 7. Histograms of a) the lifetime in days, b) the pathway length of trajectory in km, c) the mean nonlinearity parameter (nondimensional units) and d) the intensity (nondimensional units) of the long-lived anticyclones and cyclones in the Kuril Basin.

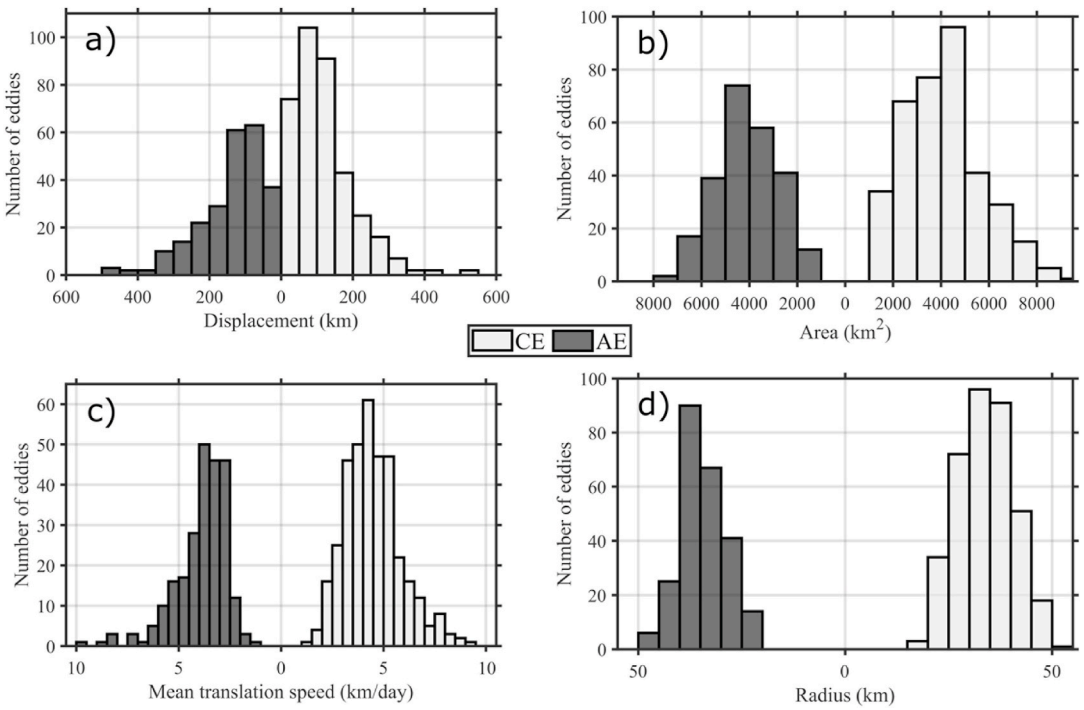

Fig. 8. Histograms of a) the displacement of the eddy's centers in km, b) the area in squared km, c) the mean propagation speed in km/day and d) the mean radius in km for the long-lived anticyclones and cyclones in the Kuril Basin.

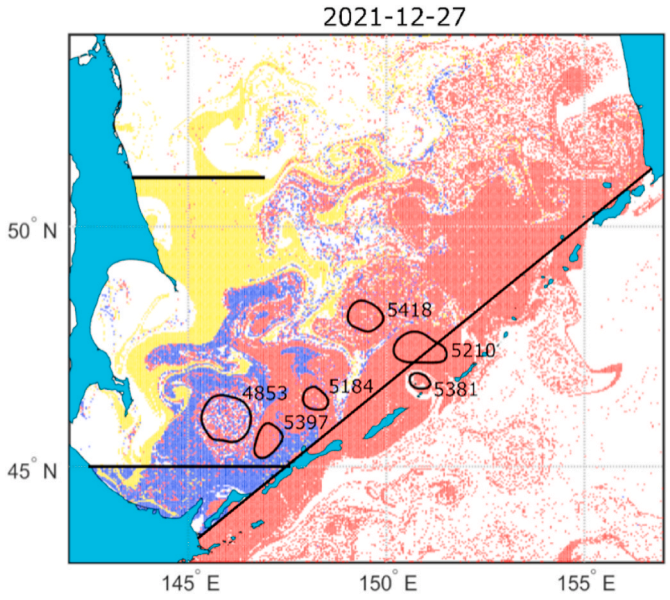

Fig. 9. The origin map on December 27, 2021 shows, as an example, spatial distribution of the three water masses in the southern Okhotsk Sea. Red color marks the open-ocean water that crossed in the past the diagonal segment with coordinates (43°N, 145.5°E and 51.75°N, 157.5°E), yellow color marks the East Sakhalin Current water that crossed the zonal segment with coordinates (45°N, 142.4°–147.6°E) and the blue color marks the Soya Warm Current water that crossed the zonal segment with coordinates (51°N, 143°–147°E). The 'white' color codes the particles that either did not cross one of the indicated segments during one year prior the date indicated on the map or because one year was not long enough to do that. The contours of a few detected eddies with their numbers are shown.

water masses, the float and GLORYS12V1 profiles were compared with the origin maps on the same dates showing the spatial distribution of the water masses in the OS.

The temperature profiles in the vortex contour of the anticyclone #2937 in the southwestern KB in the spring of 2008 are shown in Fig. 11 in the AVISO and GLORYS12V1 velocity fields (Fig. 11a and b). This eddy on the day of sampling was filled mainly with a mix of the East Sakhalin Current 'yellow' water and the open-ocean 'red' water (Fig. 11c). The temperature (Fig. 11d) and salinity profiles and TS-diagram in Fig. 9S in Supplementary material show the cold and low-salinity surface water as a result of the spring ice melting.

The results for the cyclone #3951 in the central KB sampled by a profiling float on September 6, 2015 are shown in Fig. 12. The altimetry-based origin map shows that this eddy was filled by the open ocean 'red' water with a small fraction of the 'yellow' East Sakhalin Current water. In contrast to the almost homogeneous temperature profiles for the AE #2937, the T and S profiles and T-S diagrams (see also Fig. 10S in Supplementary material) are typical of the subarctic water.

The results for the anticyclone #3335 in the southern KB sampled by a profiling float on October 5, 2011 is shown in Fig. 13. This eddy was filled with a mix of the open ocean 'red' water and the Soya Warm Current 'blue' water (Fig. 13c). The thermohaline characteristics of this AE resemble those for the CE #3951 (see also Fig. 11S in Supplementary material).

Thus, the results of Figs. 11–13 suggest that the O-maps represent the actual situation of the water masses transported within the various eddies. The results of the comparison between the thermohaline properties of eddies from these profiling floats and from GLORYS12V1 is also provided in Sec. 4.3.

To complement our analysis of O-maps, we provided time series of the seasonal variations of the different water mass fractions within the eddies' cores in Fig. 14. The confidence intervals were calculated separately for every day and the sample size was determined to count the number of vortex contours on every date in 1993-2021. The results of this figure are discussed in Sec. 4.3.

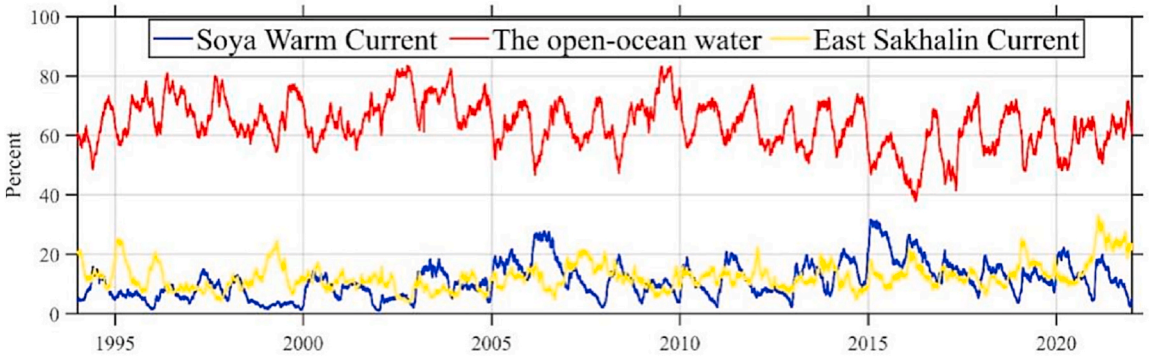

Fig. 10. The variations of fraction of the surface open ocean (red), East Sakhalin Current (yellow) and Soya Warm Current (blue) waters in the Kuril Basin limited by the 3000 m isobath in 1994–2021.

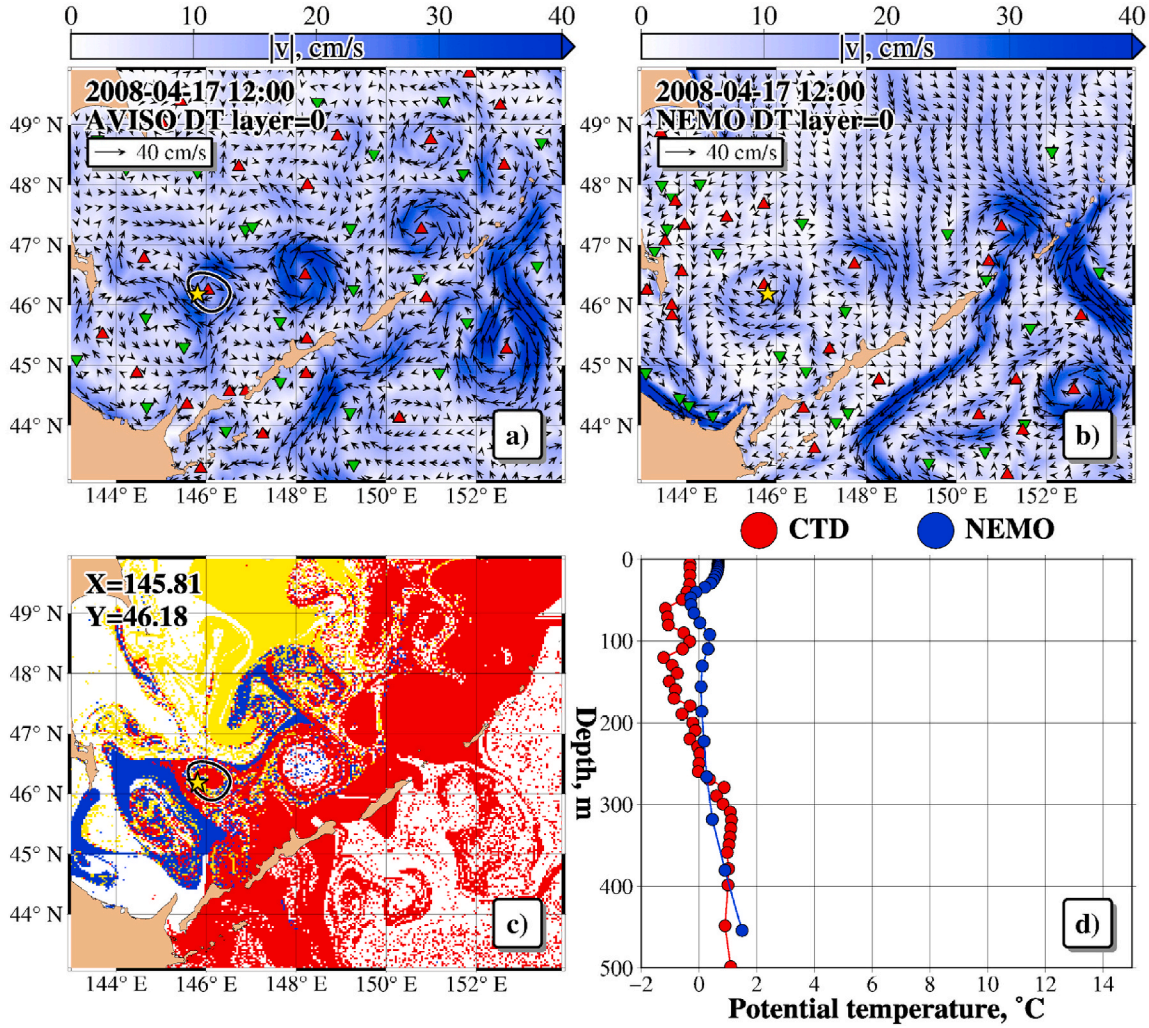

Fig. 11. a) The AVISO and b) GLORYS12V1 surface velocity fields with the anticyclone #2973 centered at 46.18°N, 145.81°E in the southwestern Kuril Basin sampled by a profiling float (star) on April 17, 2008. c) The altimetry-based origin map shows that this eddy was filled with a mix of the East Sakhalin Current 'yellow' water and the open-ocean 'red' water (the vortex contour is shown). d) The temperature profiles provided by the float (red dots) and the GLORYS12V1 reanalysis data (blue dots) on the same day. The legend of colors in panel c) is the same as in Fig. 9.

4. Discussion

4.1. Spatial distribution of eddies

The first striking observation is a dominance of long-lived CEs over AEs in the KB with the lifespan exceeding 30 days (Table 1). By the common opinion, AEs are dominant features in the KB (Wakatsuchi and Martin, 1990, 1991; Rogachev, 2000; Ohshima et al., 2002; Ohshima et al., 2005; Pishchalnik et al., 2017). This impression is due, probably, to a larger horizontal size (Fig. 8d) and amplitude of AEs as compared to CEs that makes it easier to observe anticyclones in the sea-level field. However, nobody performed a census of KB eddies for such a long period

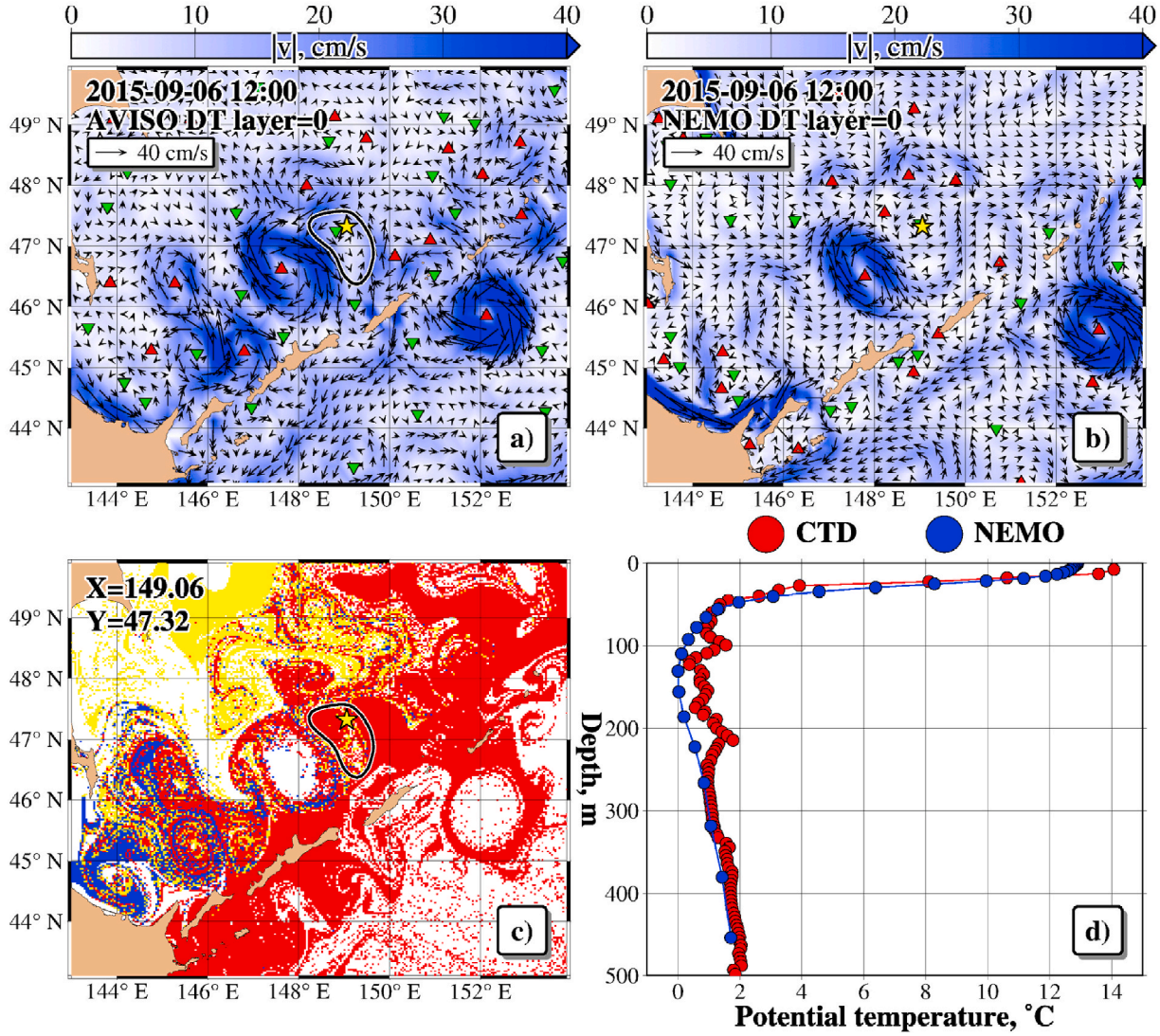

Fig. 12. a) The AVISO and b) GLORYS12V1 surface velocity fields with the cyclone #3951 centered at 47.32°N, 149.06°E in the central Kuril Basin sampled by a profiling float (star) on September 6, 2015. c) The altimetry-based origin map shows that this eddy was filled with a mix of the open ocean 'red' water with a small fraction of the 'yellow' East Sakhalin Current water (the vortex contour is shown). d) The temperature profiles provided by the float (red dots) and calculated using GLORYS12V1 reanalysis data (blue dots).

of time as it is done in this study.

As to the whole OS, CEs tend to prevail over AEs as the lifetime of eddies increases (Table 1). One of the reasons for the AE/CE disparity is the rarer occurrence of splitting events for AEs than for CEs. The stability of AEs is supported, partly, by the dominant anticyclonic circulation in the KB (Wakatsuchi and Martin, 1991; Ohshima et al., 2002; Nakamura et al., 2012; Mensah et al., 2019). We have found 368 CE splitting events against 342 AE splitting events. Moreover, trains of small-scale cyclones are often observed around large-scale anticyclones, especially around quasi-stationary ones. It has been observed earlier for some Bussol, Hokkaido and Kamchatka quasi-stationary anticyclones (Prants et al., 2016, 2018, 2020). Such a configuration stabilizes anticyclones (see, e. g., Carton, 1992) and increases the total number of small-scale cyclones. Inspection of the daily Lagrangian maps and AMEDA data confirms this statement for quasi-stationary AEs.

The second striking observation is that the long-lived eddies are not evenly distributed over the KB (Figs. 4 and 5). A few areas with increased values of the occurrence frequency have been found for each type of eddies. Such areas, highlighted in Figs. 4 and 5, are not necessary the locations where the eddies were born. As it follows from the calculation of this frequency (see Sec. 3.2), they are just the areas with increased probability to observe AEs or CEs.

As far as we know, CTD sampling has been carried out only for AEs in the KB and the adjacent areas (Wakatsuchi and Martin, 1991; Rogachev, 2000; Ohshima et al., 2005). We refer to two large domains in the KB with increased probability to observe AEs, where these samplings have been carried out, as the 'Bussol' and 'the central KB' areas (Figs. 1 and 4). The eddies there are referred as 'the seaside Bussol AEs' (in order to differentiate them from 'the ocean-side Bussol eddies' reviewed recently by Prants, 2021) and 'the deep-sea AEs'. The sampled eddies had a deep cold layer down to 700–900 m with the lower border of the cold layer, defined as the depth of 2 °C isotherm (Rogachev, 2000).

As a partial validation of the detected features of coherent eddies, we refer to the trajectories of ARGOS drifters within anticyclonic circulations (see Ohshima et al., 2002). The location of these trajectories coincides well with the areas of increased occurrence frequency of long-lived AE that was detected in our study. One of the drifters has been trapped from 7 October to 14 November of 1999 by the Bussol AE centered approximately at 47.5°N, 151°E. This cold-core eddy with the diameter of ~100 km was clearly visible in the AVHRR images in October in which a cold-core deep-sea AE was also present. The hydrographic measurements across a Bussol AE have been carried out on

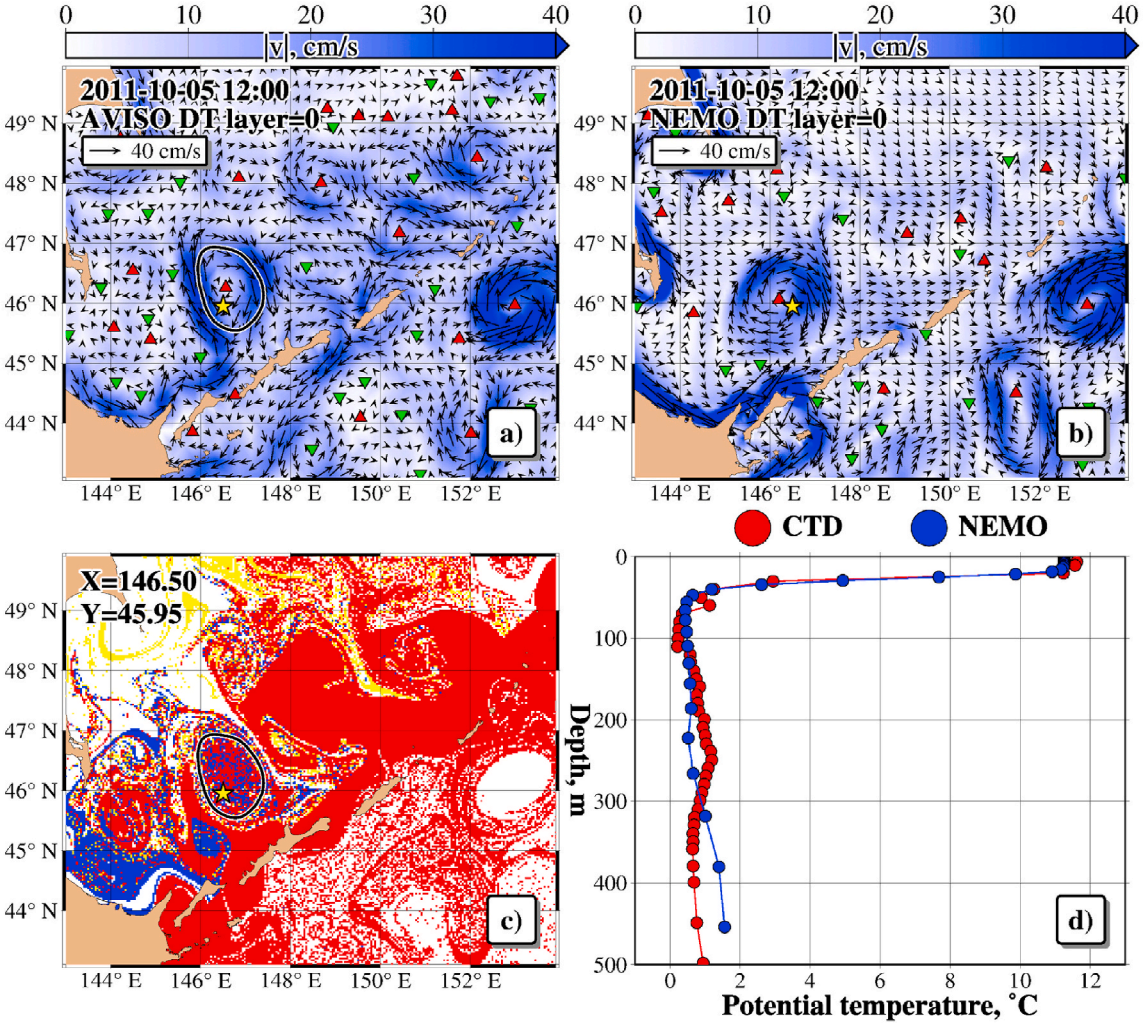

Fig. 13. a) The AVISO and b) GLORYS12V1 surface velocity fields with the anticyclone #3335 centered at 45.95°N, 146.50°E in the southern Kuril Basin sampled by a profiling float (star) on October 5, 2011. c) The altimetry-based origin map shows that this eddy was filled with a mix of the open ocean 'red' water and the Soya Warm Current 'blue' water (the vortex contour is shown). d) The temperature profiles provided by the float (red dots) and calculated using GLORYS12V1 reanalysis data (blue dots).

September 1 and 2, 1999 by Ohshima (2005). The eddy had a cold, less saline and less dense core extending to the depth of ~1200 m, with the isopycnals pointing downward towards the center. This density pattern produced the anticyclonic motion from the surface to ~800 m depth. The eddy structure was similar to that reported by Bulatov et al. (1999).

In November and December 1993, another drifter #15371 made counterclockwise loops around eddy-like cyclonic features (see Thomson et al., 1997) exactly at the same place where we have found increased occurrence frequency of the long-lived cyclones (see Fig. 5).

AEs have been regularly observed (e.g., Ebuchi, 2006) the ten-year records (1992–2001) of the sea level anomaly at the locations with increased occurrence frequency (see Figs. 4–6), i.e., at the positions of the seaside Bussol eddies and deep-sea eddies (centered at 46°N, 146°E). The diameter of the latter eddies was estimated to be 130 km on average, and they did not appear to move either away from or to any direction in the central KB with high occurrence frequency (Figs. 4 and 6).

Some eddies form when an inflow of a low-density water intrudes into the deep KB. The AEs, forming outside the KB to the east and south off the Cape Aniva and off the Shiretoko Peninsula (Fig. 1), are likely to be eddies of this type. A large number of AEs form and decay in these areas (Fig. 2), but only a few were able to enter the KB (Fig. 4a). The similar densities of formation and decay sites in the same area mean that these eddies form, stagnate and decay in the restricted area. The Shiretoko AEs have been found to contain warm, saline water near the surface, down to about 100 m deep, riding on a cold, less saline core. Comparing Figs. 2 and 4, we may conclude that the Shiretoko AEs are short-lived.

Using an eddy-resolving numerical model of circulation, Uchimoto et al. (2007) successfully represented the formation of AEs in late summer when the warm and saline Soya Warm Current water reaches the tip of the Shiretoko Peninsula in July (Fig. 6a and 7a in Uchimoto et al., 2007) and begins to swirl with the appearance of an AE around the point with coordinates 145.5°E, 44.5°N. The water of this current is not transported through Straits downstream but remains in the area near the Shiretoko Peninsula, so that a modelled anticyclone grows there gradually (Fig. 6b and 7b in Uchimoto et al., 2007). The Shiretoko eddy formation depends upon the transport of the Soya Warm Current. When the transport is small, a distinct eddy does not form. As the transport increases, the eddy appears with a diameter up to about 80 km. These findings agree with our observation of increased occurrence frequency of the short-lived AEs around the Shiretoko Peninsula (Fig. 2) and for the long-lived KB eddies (Fig. 4). Due to melting of sea ice, vertical mixing in winter and seasonal upwelling, waters in the Shiretoko region are rich in nutrients, and the Shiretoko eddies may trap nutrient rich water supporting a rich and diverse marine ecosystem (Sakurai, 2007).

Another area with increased occurrence frequency is located to the

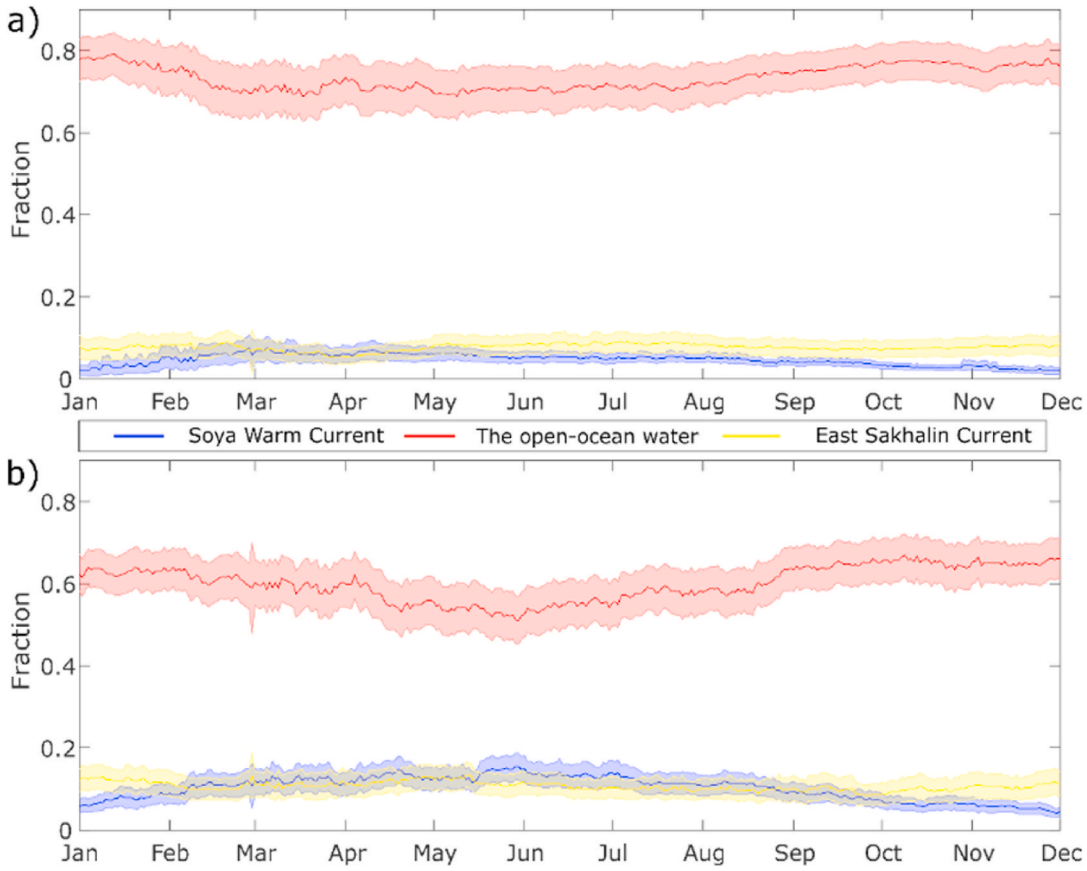

Fig. 14. The seasonal variations of the fraction of the open ocean (red), East Sakhalin Current (yellow) and Soya Warm Current (blue) waters within the surface cores of the long-lived a) AEs and b) CEs in the Kuril Basin. The data with the 95% confidence interval were calculated using the AVISO/CMEMS altimetry product.

east off Terpeniya Bay (Fig. 1) where the short-lived (Fig. 2) and long-lived (Fig. 4) AEs form regularly (see, e.g., Pishchalnik et al., 2017). Some of these eddies reach the KB being advected by the East Sakhalin Current. The AEs, forming to the east off the Cape Aniva (Fig. 1), are also connected with the East Sakhalin Current, but none of these eddies could reach the KB over the entire observation period. The AE to the east off the Terpeniya Bay has been sampled in fall of 2006 by Shevchenko et al. (2020) at the place with increased occurrence frequency in Fig. 2. As far as we know, Aniva eddies have not been sampled. In spite of the dominance of CEs over AEs, literature on CEs in the KB is practically absent.

As to the eddies without lifespan constraint, the highest densities of the formation and decay sites have been observed outside the KB, on the seaside of the Kuril Islands between the coast and 3000 m isobath (Figs. 2 and 3). In contrast to that, only a few long-lived eddies over the 29 years period were able to reach the KB from this area (Fig. 4a and 5a). Therefore, a majority of AEs and CEs formed and decayed there, and only a minority of them were able to reach the KB. It is known that potential vorticity fronts are formed along an island chain due to the spatial variation in the strength of vertical mixing. Such fronts spawn various instabilities and associated eddies (e.g., Pedlosky, 1987). The frontal eddies should contain low potential vorticity water in their cores, and thus anticyclonic eddies are easier to produce. The tidally-induced potential vorticity fronts along the Kuril Islands have been investigated numerically by Nakamura and Awaji (2004) and by Ohshima (2005). These authors simulated mesoscale and submesoscale baroclinic eddies forming on both sides of the Kuril Straits. In the mature phase, the disturbances have grown large enough that some eddies pinched off and advected offshore to the west. The pinched-off eddies were dominantly anticyclonic ones (Ohshima et al., 2005), extending from the surface to the depth of ~1200 m. Typical eddy scale and westward model propagation speed have been found to be ~100 km and ~0.6 km/day. Contrary to the model findings, we have not observed a dominance of AEs formed in this area. The numbers of AEs and CEs formed there are approximately the same (Fig. 2a, 3a and 4a and 5a).

4.2. *Kinematic characteristics of the basin eddies and comparison with the open-ocean eddies*

The kinematic characteristics of the long-lived KB eddies are discussed in this section in comparison with mesoscale eddies on the ocean side of the Kuril Islands which we call hereafter 'Kuril eddies'. The Kuril eddies form and propagate between the coastline and the deep Kuril-Kamchatka Trench, being advected by the comparatively strong East Kamchatka and Oyashio currents (Fig. 1). They typically contain the same water masses as KB eddies: the subarctic water, OS water and transformed subtropical Soya Warm Current water for eddies near the southern Kurils. Using altimetry data from 1993 to 2021, the mesoscale long-lived Kuril eddies have been detected by Udalov et al. (2023) with the help of the same automatic eddy tracking algorithm (AMEDA) as in the present study along with calculation of their kinematic characteristics.

Table 2
Comparison of the Basin eddies with the open-ocean Kuril eddies.

	Kuril Basin eddies		Kuril eddies	
	AE	CE	AE	CE
Mean lifespan (day)	203	123	117	106
Median values of lifespan (day)	146	96	67	74
Mean translation speed (km/day)	3.86	4.48	5.01	5.2
Mean values of the displacement (km)	136	118	177.5	149

In Table 2 we collected some kinematic characteristics of both types of the eddies. Among the Kuril eddies, 12.3% (3.2%) of the anticyclones and 6.4% (1%) of the cyclones lived more than one (two years). The numbers of very long-lived AEs and CEs in the KB with the lifetime exceeding 300 days are 44 and 27, respectively, with the percentage of such eddies equal to 18% for AEs and 7.3% for CEs. AEs in the KB typically live longer than CEs. They are more stable compared to CEs, like the anticyclones in the northwestern Pacific Ocean (Kaneko et al., 2015;Budyansky et al., 2022b ; Prants, 2021; Udalov et al., 2023). The KB eddies are more slowly moving objects as compared to the Kuril eddies and other trench eddies in the Western Subarctic Gyre (see Kitano, 1975; Itoh and Yasuda, 2010; Kaneko et al., 2015; Prants et al., 2018, 2020; Prants, 2021). This is due to the absence of strong currents in the KB. The radius and intensity of the KB eddies (Fig. 8d and 7d) are also smaller, in average, than those values for the Kuril eddies (Udalov et al., 2023).

By tracking daily trajectories of the centers of the long-lived KB eddies, we can follow over which depth they prefer to move. The histograms in Fig. 3S in Supplementary material demonstrate that majority of AEs and CEs move over the deepest part of the Basin (between 3000 and 3500 m) which serves as a kind of a trap for the topographically-constraint KB eddies.

4.3. The thermohaline properties and water mass fractions in the surface layer of the Kuril basin eddies

Fig. 9 shows the typical spatial distribution of water masses in the southern OS originated from the open ocean, East Sakhalin and Soya Warm currents. The origin of water was specified after crossing the corresponding segments (shown in this figure) by the particles covering initially the whole OS (see Sec. 2.2 for the computation procedure). The red particles on the ocean side of the Kuril Islands are those ones that exit the OS mainly through the southern straits in accordance with earlier observations and simulation (e.g., Fayman et al., 2021 and references therein). The fraction of water of the Soya Warm Current origin in the KB is small, but this water could reach the central KB to take part in the formation remote eddies.

Fig. 10 shows variations of the fraction of each water mass in the KB limited by the 3000 m isobath in 1994–2021. The fraction of open ocean water changes periodically in time with an increase in the cold season of a year (October–April). The fractions of Soya Warm Current and East Sakhalin Current waters vary more or less periodically but with a more erratic component. In accordance with the fractions of these water masses in the KB, both AEs and CEs contained mainly the open ocean water in their interiors (see Fig. 14). In the cold season, an increased fraction of this water is observed within the AE cores as compared with the fractions of the other two water masses due to intensification of the East Kamchatka Current and winter intensification of inflow of the western subarctic water to the OS through the northern Kuril straits (Qiu, 2001; Ohshima et al., 2002; Kida and Qiu, 2013; Prants et al., 2020; Fayman et al., 2021; Shu et al., 2021).

In the warm season (May–September), the fraction of the ocean water within CEs decreased as compared with AEs, whereas the fractions of the other water masses increased. As it follows from Fig. 5, there exists an area with increased CE occurrence frequency in the southern part of the KB, where CEs have more chances to trap Soya Warm Current and East Sakhalin Current waters. The increased fraction of the East Sakhalin Current and the Soya Warm Current waters in AEs in the cold season is due to the intensification of these currents (e.g. Fayman et al., 2020, Takizawa, 1982). Also, as small increase in the fraction of the open ocean water occurs within the core of the anticyclones just after their formation (see Fig. 4Sa in Supplementary material), which is probably due to their formation location being close to the Bussol Strait through which this water enters the sea. In contrast, we note that none of the fractions change significantly within CEs during their lifecycle (see Fig. 4Sb in Supplementary material).

A prominent phytoplankton bloom occurs in spring in the southwestern KB as well as over the continental shelf region. Close relationship between the phytoplankton bloom and sea ice melt was shown in several studies (e.g., Sorokin and Sorokin, 1999). The simulations suggest that most of the sea ice with iron-containing sediment and ice algae that melts in spring in the western KB originates from the Terpenia Bay and Sakhalin polynyas (Kuga et al., 2023). After melting there, the sea ice releases the materials that could induce a spring bloom in the Terpenia Bay and in the southernmost OS (see Fig. 1 by Kuga et al., 2023) where we have found increased occurrence frequency of eddies (Figs. 2–5). Both AEs and CEs have large values of the nonlinearity parameter (Fig. 7c) implying that they can transport not only heat, salt and potential vorticity but biochemical tracers, such as nutrients and phytoplankton. The eddies, formed in spring in these productive areas, and drifting towards the Basin could transport a nutrient rich water to oligotrophic areas creating favorable conditions for marine ecosystems and sustainable fishery industry there. Eddies provide an important enrichment mechanism in the nitrogen-limited KB waters containing productive open ocean and East Sakhalin Current waters (see Figs. 9, 10 and 13).

Let us now compare the simulated results with the actual data from the profiling floats, deployed in the OS (see Figs. 11–13 and Fig. 9S, 10S and 11S in Supplementary material). We selected some floats trapped by a few long-lived typical AEs and CEs in different parts of the KB to obtain the T/S vertical profile within these eddies. These profiles are compared with the profiles calculated from the GLORYS12V1 reanalysis data. The eddies have been identified using the AMEDA algorithm. It should be noted that the locations of the selected eddies in the AVISO and GLORYS12V1 velocity fields approximately coincide with each other. So, we are sure that the selected eddies are real eddies with the floats inside their cores.

The point is to establish a correlation (if any) between the thermohaline properties of the selected eddies and the origin maps showing the spatial distribution of the water masses in the OS. Figs. 11–13 and Fig. 9S, 10S and 11S in Supplementary material show that this correlation really exist, at least qualitatively. The T-S profiles in the vortex contour of the AE #2937 in the southwestern KB in the spring of 2008 (Fig. 11 and 9S in Supplementary material) show the cold and low-salinity surface water as a result of the spring ice melting. This is consistent with the O-map (Fig. 11c) showing that this eddy on the day of sampling was filled mainly with a mix of the East Sakhalin Current 'yellow' water and the open-ocean 'red' water. On the other hand, the CE #3951 in the central KB, sampled by a profiling float on September 6, 2015 (Fig. 12), was filled by the open-ocean 'red' water with a small fraction of the 'yellow' East Sakhalin Current water. The temperature and salinity vertical profiles and T-S diagrams of this eddy are typical of the subarctic water (see also Fig. 10S in Supplementary material). The anticyclone #3335 in the southern KB, sampled by a profiling float on October 5, 2011, was filled with a mix of the open-ocean 'red' water and the Soya Warm Current 'blue' water (Fig. 13c). The thermohaline characteristics of this AE resemble those for the CE#3951 (see also Fig. 11S in Supplementary material).

4.4. Remarks on the difference between the detected eddies and low-frequency waves

There has been a long debate about whether the observed SSH anomalies are coherent eddies or low-frequency Rossby-like waves (see, e.g., Chelton et al., 2011; Mensah and Ohshima, 2020; Gnevyshev et al., 2021; Cao et al., 2022). Satellite altimeters are the only tool that provides a global picture of these features. Mesoscale eddies are isolated and closed circulations, while Rossby waves consist of several crests and troughs perpendicular to the phase propagation direction across the whole basin.

We focused in this paper on mesoscale features in the KB in the area deeper than 3000 m. This isobath is far away from the shelf regions in

the southern OS along which arrested (trapped) topographic waves may occur. The amplitude of these waves is expected to decrease exponentially with increasing offshore distance. Mensah and Ohshima (2020) have conducted a complex empirical orthogonal function analysis based on SSHA dataset and have found that a largest part of the energy was concentrated along the shelf regions from Sakhalin Island to the Kuril Islands. Both seasonal and interannual variations of this mode correlated with the alongshore wind stress and have been explained by an arrested topographic wave.

The formation sites of the mesoscale features, we detected, are distributed in the area far away from any coast (Figs. 4 and 5), and they have no clear seasonal pattern being evenly distributed over the months in a year (see Fig. 2S in Supplementary material). The following arguments allow us to conclude that the majority of the detected mesoscale features in this study are coherent eddies demonstrating the properties that distinguish them from large-scale low-frequency waves (compare Figs. 4 and 5 in the present paper and Fig. 6a in Mensah and Ohshima, 2020).

Firstly, nonlinear coherent eddies are capable of transporting large volumes of water within the eddy interior that is advected over a long distance. Around of 98% of the detected AEs and CEs have the nonlinearity parameter $\eta > 1$. The larger the value of η, the higher the nonlinearity of eddies. We computed locations of the elliptic points and shown that they were really located in the centers of all detected mesoscale long-lived eddies. The elliptic points could be identified only for the eddies with $\eta > 1$. That means that a large majority of AEs and CEs are coherent features transporting water. The greater the value of η, the longer the time the eddy preserves a compact material entity. The value of $\eta \sim 1$ is a rough threshold below which eddies cannot transport mass even for a short time.

Secondly, we tracked Lagrangian particles (transporting a tracer) placed initially inside the surface cores of some long-lived nonlinear eddies in the KB. The examples in Fig. 5S and 6S demonstrate that a large amount of the particles is advected inside the eddies over a long distance during a long time. That means that these AEs and CEs both in the central KB and its periphery are propagating coherent Lagrangian eddies, not quasi-standing or propagating low-frequency waves (see also Sec. 4 in Supplementary material).

The patterns of current fields in eddies and in low-frequency waves are different, at least, for the waves extending over a large meridional span. Horizontal ellipses of currents in a wave are meridionally stretched, whereas they are almost circular in an eddy with zero speed at the center, the maximum swirl speed at a radius R_{max} and decreasing speed further to the periphery (see Sec. 2.1), the characteristics we have found for all detected eddies using AMEDA. The characteristic contours of the majority of the detected mesoscale features have been found to be almost circular.

As a partial validation of the detected features as coherent eddies, we may also indicate on trajectories of drifters with anticyclonic and cyclonic circulations (see Ohshima et al., 2002; Thomson et al., 1997) exactly at the same places where we have found increased occurrence frequency of the long-lived anticyclones in the KB (Figs. 4 and 5). (See Sec. 4.1). The features in these areas have been sampled by Wakatsuchi and Martin (1990), 1991, Rogachev (2000); Pishchalnik et al. (2017). The CTD sampling indicated without doubt on the vortex nature of the sampled features.

Nevertheless, we recognize that the difference between Rossby waves (especially nonlinear waves) or Rossby Normal Mode and eddy signals remains problematic and deserves further study in the OS and in other seas and oceans.

4.5. *On the limitations and advantages of the Lagrangian methodology*

In the Lagrangian approach, trajectories for a large number of virtual passive particles are calculated solving advection equation (1) in a given velocity field. Inevitable imperfections of the altimetry-based velocity field or in the velocity fields, generated by numerical circulation models is the main reason of the errors in Lagrangian simulation. These fields have enough horizontal resolution in order to resolve mesoscale features on which we focus in this study.

The AVISO velocity field and outputs of the circulation models are approximations to the 'real' velocity field in the ocean that is impossible to know exactly. Our estimates of the fractions of different water masses in the OS (Fig. 9) and in the vortex cores (Figs. 10 and 14) are based not on individual trajectories but on hundreds of thousands of particles. We cannot guarantee that we compute 'true' trajectories of individual particles, which may be very complicated or even chaotic. However, the shadowing lemma in the theory of dynamical systems (see, e.g., Ott, 2002) states that every numerically computed trajectory in a 'strongly' chaotic system stays close to a 'true' trajectory with a slightly altered initial position. That means that the estimates of the fraction of different water masses are statistically significant just because they are based on a very large number of advected particles. In spite of the limitations of the Lagrangian simulation, this is the only way to estimate fractions of distinct water masses in different sea and oceans (see e.g., the Kuroshio-Oyashio frontal zone (Prants et al., 2018; Nishikawa, 2021; Udalov et al., 2023), the Bering Sea (Prants et al., 2019), the Lofoten Basin (Fedorov et al., 2021), Barents Sea (Novoselova et al., 2023), the Benguela upwelling zone in the Atlantic Ocean (Belonenko et al., 2024) and in other regions).

As any eddy detection and tracking algorithm, AMEDA has some drawbacks in detecting eddies. We cannot exclude that some of the detected eddies are not coherent eddy-like features as the one shown in Fig. 7S. However, each such case should be considered individually tracking not only the corresponding AMEDA contours, but also inspecting daily Lagrangian maps and computing transport of a tracer within the vortex core as it was done in Fig. 7S. We tracked visually the daily AMEDA vortex contours and inspected daily elliptic points on the Lagrangian maps for all the KB eddies lasting for more than 600 days and have found that all these eddies existed as coherent entities during their lifecycle (see Sec. 4 in Supplementary material and Fig. 8S). The fraction of these eddies is rather small in the total statistics of the KB eddies, not exceeding 2%.

5. Conclusions

The spatial distribution, occurrence frequency, kinematic and dynamic properties of mesoscale eddies and fractions of different water masses within the surface cores have been studied in the deep Kuril Basin of the Okhotsk Sea based on altimetry data during 1993–2021. The main attention was paid to long-lived eddies which spent more than 30 days in the Kuril Basin. Using the automatic eddy tracking algorithm AMEDA, we conducted the first systematic census of the long-lived anticyclonic and cyclonic eddies in the altimetry era. A few areas with increased values of the occurrence frequency have been found for each type of eddies, mainly in the eastern and southern parts of the Basin and adjacent areas, in accordance with satellite-based observations and samplings. Both the AEs and CEs often formed on the seaside of the Bussol Strait and in the central KB. They typically contain the same waters as mesoscale eddies on the ocean side of the Kuril Islands and over the Kuril-Kamchatka trench (Udalov et al., 2023). The KB eddies are more slowly moving objects as compared with the Kuril eddies.

The detected long-lived cyclones have been found to dominate over the long-lived anticyclones partly because CEs split more often than AEs. Anticyclones, typically, are larger, more intense and stable as compared with cyclones. Both the anticyclones and cyclones have large values of the nonlinearity parameter implying that they can transport heat, salt, nutrients and biota. 44 AEs and 27 CEs had the lifetime exceeding 300 days and with the trajectory pathway length exceeding 1000 km whereas the displacements of their centers rarely exceeding 300 km. That means that the long-lived KB eddies circulated in a restricted area.

We have estimated for the first time the fractions of water of different

origin within the surface cores of the basin eddies using the proposed particle-tracking methodology. That allowed us to separate transformed subtropical water of the Soya Warm Current originating in the Japan Sea from the Okhotsk Sea, water of the East Sakhalin Current and subarctic Pacific water and to estimate seasonal and interannual variations of the fractions of these water masses and average temperature and salinity within the basin eddies. The fraction of the open-ocean water in the KB changes periodically in time increasing in the cold season when the Oyashio intensifies. In average, AEs and CEs contain mainly the water of the open ocean as compared with the fractions of waters of the Soya Warm Current and East Sakhalin Current with insignificant variations in time. Using historical GLORYS12V1 reanalysis data, the temperature-salinity diagrams have been found to differ for eddies with different fractions of the water masses. We plan in the future to develop an automatic downloading of the available T/S profiles for a long period of time in order to validate the estimated fractions of water masses within the cores of mesoscale eddies.

CRediT authorship contribution statement

Aleksandr Udalov: Visualization, Software. **Maxim Budyansky:** Visualization, Validation, Methodology, Data curation. **Sergey Prants:** Writing – review & editing, Writing – original draft, Supervision, Funding acquisition, Formal analysis, Conceptualization. **Aleksandr Didov:** Software, Visualization.

Declaration of competing interest

The authors declare that they have no known competing financial interests or personal relationships that could have appeared to influence the work reported in this paper.

Data availability

Data will be made available on request.

Acknowledgements

The work was supported by the Russian Science Foundation (project no. 23-17-00068) with the help of a high-performance computing cluster at the Pacific Oceanological Institute and numerical codes elaborated within the State Task No. 124022100072–5.

Appendix A. Supplementary data

Supplementary data to this article can be found online at https://doi.org/10.1016/j.dsr.2024.104374.

References

Belonenko, T.V., Budyansky, M.V., Akhtyamova, A.V., Udalov, A.A., 2024. Investigation of the Benguela upwelling eddies using Lagrangian modeling methods. Ocean Dynam. 74, 373–390. https://doi.org/10.1007/s10236-024-01609-8.

Budyansky, M.B., Kulik, V.V., Kivva, K.K., Uleysky, M.Yu, Prants, S.V., 2022a. Waters in the Sea of Okhotsk based on satellite data in application to the walley pollock fishery. Izvestiya Atmos. Ocean. Phys. 58, 1427–1437. https://link.springer.com/article/10.1134/S0001433822120088.

Budyansky, M.B., Prants, S.V., Uleysky, M.Yu, 2022b. Odyssey of aleutian eddies. Ocean Dynam 72, 455–476. https://doi.org/10.1007/s10236-022-01508-w.

Bulatov, N.V., Kurennaya, L.A., Muktepavel, L.S., Aleksanina, M.G., Gerbek, E.E., 1999. Eddy water structure in the southern Okhotsk Sea and its seasonal variability (results of satellite monitoring). Oceanology 39, 29–37.

Cao, C., Chen, G., Wang, X., 2022. How mesoscale eddies masquerade as Rossby waves in merged altimetric products. J. Geophys. Res.: Oceans 127, e2022JC018981. https://doi.org/10.1029/2022JC018981.

Carton, X.J., 1992. On the merger of shielded vortices. Europhys. Lett. 18 (8), 697–703. https://doi.org/10.1209/0295-5075/18/8/006.

Chelton, D.B., Schlax, M.G., Samelson, R.M., 2011. Global observations of nonlinear mesoscale eddies. Prog. Oceanogr. 91, 167–216. https://doi.org/10.1016/j.pocean.2011.01.002.

Ebuchi, N., 2006. Seasonal and interannual variations of the East Sakhalin Current observed by the TOPEX/POSEIDON altimeter. J. Oceanogr. 62, 171–183. https://doi.org/10.1007/s10872-006-0042-x.

Ebuchi, N., Fukamachi, Y., Ohshima, K.I., Wakatsuchi, M., 2009. Subinertial and seasonal variations in the Soya Warm Current revealed by HF ocean radars, coastal tide gauges, and bottom-mounted ADCP. J. Oceanogr. 65, 31–43. https://doi.org/10.1007/s10872-009-0003-2.

Fayman, P.A., Prants, S.V., Budyansky, M.V., Uleysky, M.Yu, 2020. New circulation features in the Okhotsk Sea from a numerical model. Izvestiya Atmos. Ocean. Phys. 56 (6), 618–631. https://doi.org/10.1134/S0001433820060043.

Fayman, P.A., Prants, S.V., Budyansky, M.V., Uleysky, M.Yu, 2021. Simulated pathways of the northwestern pacific water in the Okhotsk Sea and ocean-sea exchange transport. Izvestiya. Atmospheric and Oceanic Physics 57 (3), 329–340. https://doi.org/10.1134/S000143382103004X.

Fedorov, A.M., et al., 2021. Lagrangian modeling of water circulation in the Lofoten Basin. Dynam. Atmos. Oceans 96, 101258. https://doi.org/10.1016/j.dynatmoce.2021.101258.

Flierl, G.G.R., 1981. Particle motions in large-amplitude wave fields. Geophys. Astrophys. Fluid Dynam. 18 (1–2), 39–74. https://doi.org/10.1080/03091928108208773.

Gladyshev, S., Martin, S., Riser, S., Figurkin, A., 2000. Dense water production on the northern Okhotsk shelves: comparison of shipbased spring-summer observations for 1996 and 1997 with satellite observations. J. Geophys. Res. 105 (C11), 281–299. https://doi.org/10.1029/1999JC000067.

Gnevyshev, V.G., Malysheva, A.A., Belonenko, T.V., Koldunov, A.V., 2021. On Agulhas eddies and Rossby waves travelling by forcing effects. Russ. J. Earth Sci. 21, ES5003 https://doi.org/10.2205/2021ES000773.

Itoh, S., Yasuda, I., 2010. Water mass structure of warm and cold anticyclonic eddies in the western boundary region of the Subarctic North Pacific. J. Phys. Oceanogr. 40, 2624–2642. https://doi.org/10.1175/2010jpo4475.1.

Kaneko, H., Itoh, S., Kouketsu, S., Okunishi, T., Hosoda, S., Suga, T., 2015. Evolution and modulation of a poleward propagating anticyclonic eddy along the Japan and Kuril-Kamchatka trenches. J. Geophys. Res.: Oceans 120, 4418–4440. https://doi.org/10.1002/2014JC010693.

Katsumata, K., Yasuda, I., 2010. Estimates of non-tidal exchange transport between the Sea of Okhotsk and the North pacific. J. Oceanogr. 66, 489–504. https://doi.org/10.1007/s10872-010-0041-9.

Khen, G.V., Muktepaveln, L.P., 1995. Study of eddies in the southwestern part of the Sea of Okhotsk according to data from Meteor series of satellites. Issled. Zemli Kosmosa 4, 76–79 (abstract in English).

Kida, S., Qiu, B., 2013. An exchange flow between the Okhotsk Sea and the North Pacific driven by the East Kamchatka Current. J. Geophys. Res. Oceans 118. https://doi.org/10.1002/2013JC009464.

Kitano, K., 1975. Some properties of the warm eddies generated in the confluence zone of the Kuroshio and Oyashio currents. J. Phys. Oceanogr. 5, 245–252. https://doi.org/10.1175/1520-0485(1975)005<0245:SPOTWE>2.0.CO;2.

Kolomeytsev, V.V., 2020. Variability of the West Kamchatka current in winters of 1994–2019, by altimetry data. Izvestiya TINRO 200 (2), 412–426. https://doi.org/10.26428/1606-9919-2020-200-412-426 (abstract in English).

Kolonchin, Kirill V., Pavlova, Anna O., Betin, Oleg I., Yanovskaya, Nina V., 2022. Walleye pollock as an object of Russian and world fishery. Trudy VNIRO 189, 5–15. https://doi.org/10.36038/2307-3497-2022-189-5-15 (abstract in English).

Kuga, M., Ohshima, K.I., Kimura, N., et al., 2023. Particle-tracking experiments of coastal-origin sea ice that could induce high biological productivity in the Sea of Okhotsk. J. Oceanogr. 79, 145–159. https://doi.org/10.1007/s10872-022-00670-5.

Le Vu, B., Stegner, A., Arsouze, T., 2018. Angular momentum eddy detection and tracking algorithm (AMEDA) and its application to coastal eddy formation. J. Atmos. Ocean. Technol. 35 (4), 739–762. https://doi.org/10.1175/JTECH-D-17-0010.1.

Mancho, A.M., Small, D., Wiggins, S., 2006. A comparison of methods for interpolating chaotic flows from discrete velocity data. Comput. Fluid 35, 416–428. https://doi.org/10.1016/j.compfluid.2005.02.003.

Mensah, V., Ohshima, K.I., 2020. Variabilities of the sea surface height in the Kuril Basin of the Sea of Okhotsk: coherent shelf-trapped mode and Rossby normal modes. J. Phys. Oceanogr. 50 (8), 2289–2313. https://doi.org/10.1175/JPO-D-19-0216.1.

Mensah, V., Ohshima, K.I., Nakanowatari, T., Riser, S., 2019. Seasonal changes of water mass, circulation and dynamic response in the Kuril Basin of the Sea of Okhotsk. Deep Sea Res. Oceanogr. Res. Pap. 144 (2), 115–131. https://doi.org/10.1016/j.dsr.2019.01.012.

Mitnik, L.M., Dubina, V.A., 2019. The Sea of Okhotsk: scientific applications of remote sensing. Remote Sensing of the Asian Seas 159–175. https://doi.org/10.1007/978-3-319-94067-0_8.

Mundo, R., et al., 2023. A review of the oceanographic structure and biological productivity in the southern Okhotsk Sea. Prog. Oceanogr. 221, 103194 https://doi.org/10.1016/j.pocean.2023.103194.

Nakamura, T., Awaji, T., 2004. Tidally induced diapycnal mixing in the Kuril Straits and its role in water transformation and transport: a three-dimensional nonhydrostatic model experiment. J. Geophys. Res. 109, C09S07 https://doi.org/10.1029/2003JC001850.

Nakamura, T., Matthews, J.P., Awaji, T., Mitsudera, H., 2012. Sub-mesoscale eddies near the Kuril Straits: asymmetric generation of clockwise and counterclockwise eddies by barotropic tidal flow. J. Geophys. Res. 117, C12 https://doi.org/10.1029/2011JC007754.

Nihashi, S., Ohshima, K.I., Tamura, T., Fukamachi, Y., Saitoh, S., 2009. Thickness and production of sea ice in the Okhotsk Sea coastal polynyas from AMSR-E. J. Geophys. Res. 114, C10025 https://doi.org/10.1029/2008JC005222.

Nishikawa, H., et al., 2021. Surface water pathways in the subtropical-subarctic frontal zone of the western North Pacific. Prog. Oceanogr. 199, 102691 https://doi.org/10.1016/j.pocean.2021.102691.
Novoselova, E.V., Belonenko, T.V., Gordeeva, S.M., Budyansky, M.V., 2023. The Atlantic gateway to the Arctic in the mirror of the Kola transect. Oceanology 63 (Suppl. 1), S54–S64, 0.1134/S0001437023070123.
Ohshima, K.I., Wakatsuchi, M., Fukamachi, Y., Mizuta, G., 2002. Near-surface circulation and tidal currents of the Okhotsk Sea observed with satellite-tracked drifters. J. Geophys. Res. 107, 3195. https://doi.org/10.1029/2001JC001005.
Ohshima, K., Fukamachi, Y., Mutoh, T., Wakatsuchi, M., 2005. A generation mechanism for mesoscale eddies in the Kuril Basin of the Okhotsk Sea: baroclinic instability caused by enhanced tidal mixing. J. Oceanogr. 61 (2), 247. https://doi.org/10.1007/s10872-005-0035-1.
Ott, E., 2002. Chaos in Dynamical Systems, second ed. Cambridge University Press, Cambridge, p. 480.
Pedlosky, J., 1987. Geophysical Fluid Dynamics, second ed. Springer-Verlag, New York, p. 710.
Pegliasco, C., Delepoulle, A., Mason, E., Morrow, R., Faugère, Y., Dibarboure, G., 2022. META3.1exp: a new global mesoscale eddy trajectory atlas derived from altimetry. Earth Syst. Sci. Data 14, 1087–1107. https://doi.org/10.5194/essd-14-1087-2022.
Pishchalnik, V.M., Arkhipkin, V.S., Leonov, A.V., 2017. Modeling mean month thermohaline patterns and water circulation on southwestern shelf of Sakhalin. Izv. TINRO. 191, 160–175. https://doi.org/10.26428/1606-9919-2017-191-160-175 (abstract in Russian).
Prants, S.V., 2015. Backward-in-time methods to simulate chaotic transport and mixing in the ocean. Phys. Scripta 90, 074054. https://doi.org/10.1088/0031-8949/90/7/074054.
Prants, S.V., 2021. Trench eddies in the northwest pacific: an overview. Izvestiya Atmos. Ocean. Phys. 57 (4), 341–353. https://doi.org/10.1134/S0001433821040216.
Prants, S.V., Lobanov, V.B., Budyansky, M.V., Uleysky, M.Y., 2016. Lagrangian analysis of formation, structure, evolution and splitting of anticyclonic Kuril eddies. Deep Sea Res. I 109, 61–75. https://doi.org/10.1016/j.dsr.2016.01.003.
Prants, S.V., Uleysky, M.Y., Budyansky, M.V., 2017. Lagrangian Oceanography: Large-Scale Transport and Mixing in the Ocean, vol. 271. Springer Verlag, Berlin, New York. https://doi.org/10.1007/978-3-319-53022-2.
Prants, S.V., Budyansky, M.V., Uleysky, M.Y., 2018. How eddies gain, retain and release water: a case study of a Hokkaido anticyclone. J. Geophys. Res. 123, 2081–2096. https://doi.org/10.1002/2017jc013610.
Prants, S.V., Andreev, A.G., Uleysky, M.Y., Budyansky, M.V., 2019. Lagrangian study of mesoscale circulation in the Alaskan Stream area and the eastern Bering Sea. Deep Sea Research II 169–170, 104560. https://doi.org/10.1016/j.dsr2.2019.03.005.
Prants, S.V., Budyansky, M.V., Lobanov, V.B., Sergeev, A.F., Uleysky, M.Y., 2020. Observation and Lagrangian analysis of quasi-stationary Kamchatka trench eddies. J. Geophys. Res. 125, 1–21. https://doi.org/10.1029/2020JC016187.
Prants, S.V., Fayman, P.A., Budyansky, M.V., Uleysky, M.Y., 2022. Simulation of winter deep slope convection in peter the great bay (Japan sea). Fluid 7, 134. https://doi.org/10.3390/fluids7040134.
Qiu, Bo, 2001. Kuroshio and Oyashio currents. Encyclopedia of Ocean Sciences. Academic Press, pp. 1413–1425.
Rabinovich, A.B., Thomson, R.E., Bograd, S.J., 2002. Drifter observations of anticyclonic eddies near Bussol' strait, the Kuril islands. J. Oceanogr. 58, 661–671. https://doi.org/10.1023/A:1022890222516.
Rogachev, K.A., 2000. Recent variability in the Pacific western subarctic boundary currents and Sea of Okhotsk. Prog. Oceanogr. 47, 299–336. https://doi.org/10.1016/S0079-6611(00)00040-9.
Sakurai, Y., 2007. An overview of the Oyashio ecosystem. Deep-Sea Research II 54, 2526–2542. https://doi.org/10.1016/j.dsr2.2007.02.007.
Shcherbina, A.Y., Talley, L.D., Rudnick, D.L., 2003. Direct observations of North Pacific ventilation: brine rejection in the Okhotsk Sea. Science 302, 1952–1955. https://doi.org/10.1126/science.1088692.
Shevchenko, G.V., Chastikov, V.N., Tsoy, A.T., 2020. Eddies off the southeastern coast of Sakhalin island. Geosystems of Transition Zones 4 (1), 35–45. https://doi.org/10.30730/2541-8912.2020.4.1.035-045 (In Russian).
Shu, H., Mitsudera, H., Yamazaki, K., Nakamura, T., Kawasaki, T., Nakanowatari, T., Nishikawa, H., Sasaki, H., 2021. Tidally modified western boundary current drives interbasin exchange between the Sea of Okhotsk and the North Pacific. Sci. Rep. 11, 12037. https://doi.org/10.1038/s41598-021-91412-y.
Sorokin, Y.I., Sorokin, P.Y., 1999. Production in the Sea of Okhotsk. J. Plankton Res. 21, 201–230. https://doi.org/10.1093/plankt/21.2.201.
Stegner, A., Le Vu, B., Dumas, F., Ghannami, M.A., Nicolle, A., Durand, C., Faugere, Y., 2021. Cyclone anticyclone asymmetry of eddy detection on gridded altimetry product in the Mediterranean Sea. J. Geophys. Res.: Oceans 126, e2021JC017475. https://doi.org/10.1029/2021JC017475.
Stepanov, D.V., 2017. Estimating the baroclinic Rossby radius of deformation in the Sea of Okhotsk. Russ. Meteorol. Hydrol. 42 (9), 601–606. https://doi.org/10.3103/S1068373917090072, 2017.
Takizawa, T., 1982. Characteristics of the Soya warm current in the Okhotsk Sea. J. Oceanogr. Soc. Jpn. 38, 281–292. https://doi.org/10.1007/BF02114532.
Talley, L.D., 1991. An Okhotsk Sea water anomaly: implications for ventilation in the North pacific. Deep-Sea Res. 38A, 171–190. https://doi.org/10.1016/S0198-0149(12)80009-4.
Thomson, R.E., LeBlond, P.H., Rabinovich, A.B., 1997. Oceanic odyssey of a satellite-tracked drifter: North Pacific variability delineated by a single drifter trajectory. J. Oceanogr. 53, 81–87. https://doi.org/10.1007/BF02700751.
Uchimoto, K., Mitsudera, H., Ebuchi, N., 2007. Anticyclonic eddy caused by the Soya warm current in an Okhotsk OGCM. J. Oceanogr. 63, 379–391. https://doi.org/10.1007/s10872-007-0036-3.
Udalov, A.A., Budyansky, M.V., Prants, S.V., 2023. A census and properties of mesoscale Kuril eddies in the altimetry era. Deep-Sea Res. I 200, 104129. https://doi.org/10.1016/j.dsr.2023.104129.
Wakatsuchi, M., Martin, S., 1990. Satellite observations of the ice cover of the Kuril Basin region of the Okhotsk Sea and its relation to the regional oceanography. J. Geophys. Res. 95 https://doi.org/10.1029/JC095iC08p13393, 13,393–13,410.
Wakatsuchi, M., Martin, S., 1991. Water circulation of the Kuril Basin of the Okhotsk Sea and its relation to eddy formation. J. Oceanogr. Soc. Jpn. 47, 152–168.
Zhabin, I.A., Andreev, A.G., 2019. Interaction of mesoscale and submesoscale eddies in the Sea of Okhotsk based on satellite data. Izvestiya Atmos. Ocean. Phys. 55, 1114–1124. https://doi.org/10.1134/S0001433819090573.
Zhabin, I.A., Luk'yanova, N.B., 2011. Interaction of anticyclonic eddies with the Soya current in the southern part of the Sea Okhotsk according to satellite observation data. Issled. Zemli Kosmosa 1, 86–90 (abstract in English).